Tracking the impact of environment on the galaxy stellar mass function up to z ~ 1 in the 10 k zCOSMOS sample

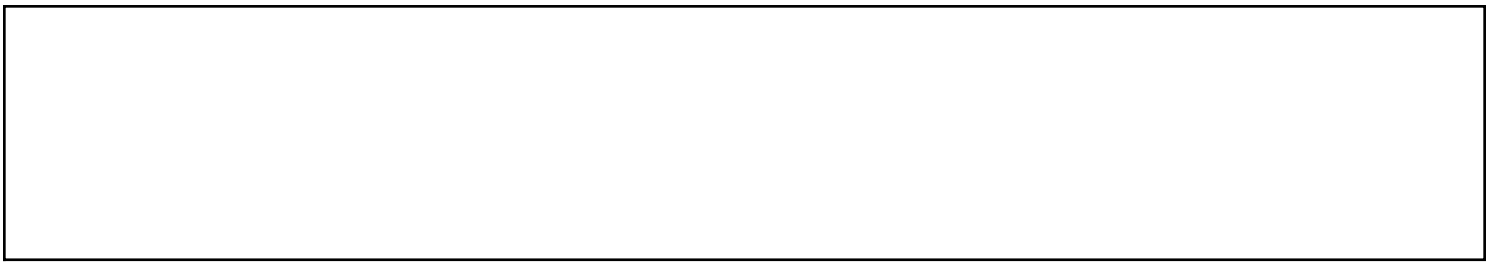

A&A 524, A76 (2010)
DOI: 10.1051/0004-6361/200912801

Astronomy & Astrophysics

Tracking the impact of environment on the galaxy stellar mass function up to $z \sim 1$ in the 10 k zCOSMOS sample⋆

M. Bolzonella[1], K. Kovač[2], L. Pozzetti[1], E. Zucca[1], O. Cucciati[3], S. J. Lilly[2], Y. Peng[2], A. Iovino[4], G. Zamorani[1], D. Vergani[1], L. A. M. Tasca[3,5], F. Lamareille[6], P. Oesch[2], K. Caputi[7,2], P. Kampczyk[2], S. Bardelli[1], C. Maier[2], U. Abbas[8], C. Knobel[2], M. Scodeggio[5], C. M. Carollo[2], T. Contini[6], J.-P. Kneib[3], O. Le Fèvre[3], V. Mainieri[9], A. Renzini[10], A. Bongiorno[11], G. Coppa[1,12], S. de la Torre[4,5], L. de Ravel[3,7], P. Franzetti[5], B. Garilli[5], J.-F. Le Borgne[6], V. Le Brun[3], M. Mignoli[1], R. Pelló[6], E. Perez-Montero[6,13], E. Ricciardelli[10,14], J. D. Silverman[2,15], M. Tanaka[9,15], L. Tresse[3], D. Bottini[5], A. Cappi[1], P. Cassata[16], A. Cimatti[12], L. Guzzo[4], A. M. Koekemoer[17], A. Leauthaud[18], D. Maccagni[5], C. Marinoni[19], H. J. McCracken[20], P. Memeo[5], B. Meneux[11,21], C. Porciani[22], R. Scaramella[23], H. Aussel[24], P. Capak[25], C. Halliday[26], O. Ilbert[3], J. Kartaltepe[27,28], M. Salvato[25,29], D. Sanders[27], C. Scarlata[25], N. Scoville[25], Y. Taniguchi[30], and D. Thompson[31]

(Affiliations can be found after the references)

Received 30 June 2009 / Accepted 21 September 2010

ABSTRACT

We study the impact of the environment on the evolution of galaxies in the zCOSMOS 10 k sample in the redshift range $0.1 \leq z \leq 1.0$ over an area of $\sim$1.5 deg^2. The considered sample of secure spectroscopic redshifts contains about 8500 galaxies, with their stellar masses estimated by SED fitting of the multiwavelength optical to near-infrared (NIR) photometry. The evolution of the galaxy stellar mass function (GSMF) in high and low density regions provides a tool to study the mass assembly evolution in different environments; moreover, the contributions to the GSMF from different galaxy types, as defined by their SEDs and their morphologies, can be quantified. At redshift $z \sim 1$, the GSMF is only slightly dependent on environment, but at lower redshifts the shapes of the GSMFs in high- and low-density environments become extremely different, with high density regions exhibiting a marked bimodality, not reproducible by a single Schechter function. As a result of this analysis, we infer that galaxy evolution depends on both the stellar mass and the environment, the latter setting the probability of a galaxy to have a given mass: all the galaxy properties related to the stellar mass show a dependence on environment, reflecting the difference observed in the mass functions. The shapes of the GSMFs of early- and late-type galaxies are almost identical for the extremes of the density contrast we consider, ranging from isolated galaxies to rich group members. The evolution toward $z = 0$ of the transition mass $\mathcal{M}_{\rm cross}$, i.e., the mass at which the early- and late-type GSMFs match each other, is more rapid in high density environments, because of a difference in the evolution of the normalisation of GSMFs compared to the total one in the considered environment. The same result is found by studying the relative contributions of different galaxy types, implying that there is a more rapid evolution in overdense regions, in particular for intermediate stellar masses. The rate of evolution is different for sets of galaxy types divided on the basis of their SEDs or their morphologies, tentatively suggesting that the migration from the blue cloud to the red sequence occurs on a shorter timescale than the transformation from disc-like morphologies to ellipticals. Our analysis suggests that environmental mechanisms of galaxy transformation start to be more effective at $z < 1$. The comparison of the observed GSMFs to the same quantities derived from a set of mock catalogues based on semi-analytical models shows disagreement, in both low and high density environments: in particular, blue galaxies in sparse environments are overproduced in the semi-analytical models at intermediate and high masses, because of a deficit of star formation suppression, while at $z < 0.5$ an excess of red galaxies is present in dense environments at intermediate and low masses, because of the overquenching of satellites.

Key words. cosmology: observations – galaxies: evolution – galaxies: fundamental parameters – galaxies: luminosity function, mass function

1. Introduction

The environmental dependence of galaxy properties (colour, star formation, mass) is well established in the local universe. At present many local studies have been carried out to analyse the influence of environment on colours, luminosities, morphologies, structural parameters, star formation, and stellar masses: all local relations can be considered as different faces of the morphology-density relation shown by Dressler (1980).

At higher redshifts, this kind of study becomes very difficult, because the need for large spectroscopic samples of faint galaxies with a good sampling rate hampers a reliable estimate of the environment. Until now, therefore, most of the studies in high density environments have analysed galaxy clusters or groups and the more general effect of the environment on field galaxy evolution remains poorly explored. The evolution of the galaxy stellar mass function (GSMF) as a function of the large-scale environment has been studied in the DEEP2 Galaxy Redshift Survey (Bundy et al. 2006), considering the redshift range $z = 0.4-1.4$, which limits the connection between this study and those in the local Universe.

Some remaining open questions are: what is the most important property leading the evolution of field galaxies? Is the fate of a galaxy decided once its mass is defined or do some external players have a role? And, if the environment plays such a role,

⋆ Based on observations obtained at the European Southern Observatory(ESO) Very Large Telescope (VLT), Paranal, Chile, as part of the Large Program 175.A-0839 (the zCOSMOS Spectroscopic Redshift Survey).

when does it start to affect galaxy evolution, and by means of which mechanism?

On the basis of literature results, the full story of galaxies is not consistently presented.

Most low-redshift studies are based on SDSS data. We try to summarise the most relevant conclusions, without pretending to be exhaustive. Some studies assert that the mass is the most important parameter in galaxy evolution: from the colour bimodality, Balogh et al. (2004) propose that the properties of star-forming galaxies are mainly related to their mass and that, to preserve the bimodality without altering the colours modelled by two Gaussian distributions, the transformation from late- to early-type galaxies should be rapid in truncating the star formation and efficient for all luminosities and environments. Analogous studies reach similar conclusions: Hogg et al. (2003) find that blue galaxies show no correlation between their luminosity/mass and local density at a fixed colour; Baldry et al. (2006) affirm that the fraction of red galaxies depends on environment, but not their colour-mass relation. Thomas et al. (2010) find that correlations between properties of galaxies in the red sequence are only driven by galaxy mass. Furthermore, van den Bosch et al. (2008b), investigating the efficiency of transformation processes on the SDSS groups catalogue, claim that both the colour and the concentration of a satellite galaxy are mostly determined by their stellar mass.

On the other hand, many other studies based on the same SDSS dataset agree on giving importance, at different levels, to both nature and nurture in the evolutionary paths of galaxies. In these studies, environment is not considered a secondary effect and it has an impact on one or more of the galaxy properties and their relations such as colour, star formation rate and its spatial variation, structural parameters, morphology, the presence of active galactic nuclei (AGN), age, and the timescale of transformation of galaxies (e.g. Kauffmann et al. 2004; Tanaka et al. 2004; Bamford et al. 2009; Skibba et al. 2009; Welikala et al. 2009; Cooper et al. 2010b; Gavazzi et al. 2010; Clemens et al. 2006; Bernardi et al. 2006; Lee et al. 2010; Mateus et al. 2007, 2008; Blanton et al. 2005a; Gómez et al. 2003).

In addition to considering the importance of the environment on galaxy evolution, the scale on which the environment is evaluated has been found to be of huge importance: for instance, another study on the colour bimodality by Wilman et al. (2010) finds that a correlation of the colour and the fraction of red galaxies with increasing densities is seen only on scales smaller than $\sim 1\,h^{-1}$ Mpc, which is the characteristic scale on which galaxies are accreted in more massive dark matter haloes, undergoing the truncation of their star formation. Other studies dealing with the groups environment support a similar scenario in which central and satellites galaxies follow different evolutionary paths, with satellite galaxies falling into more massive haloes and experiencing a slow transformation because of the removal of gas by strangulation, resulting in the fading of star formation (Rogers et al. 2010; Weinmann et al. 2009; van der Wel et al. 2009, 2010; van den Bosch et al. 2008a).

Still at low redshifts, but using 2MASS and LCRS data, Balogh et al. (2001) distinguished between different environments such as field, groups, and clusters, finding that luminosity and mass functions depend on both galaxy type (with steeper functions for emission line galaxies) and environment (with more massive and brighter objects being more common in clusters), mainly as a consequence of the different contributions of passive galaxies.

At higher redshifts, probing the effect of environment on galaxy evolution becomes more difficult and often this kind of study uses projected estimators of local density and relies on photometric redshifts (e.g. Scoville et al. 2007a; Wolf et al. 2009). The main studies using spectroscopic redshifts analyse data from the two major surveys of the recent past, DEEP2 (Davis et al. 2003) and VVDS (Le Fèvre et al. 2003).

Bundy et al. (2006), using DEEP2 data at $0.4 < z < 1.4$ and $R_{\rm AB} < 24.1$, estimate the effect of environment on GSMFs: they drew the conclusion that the quenching of star formation, and then the transition between the blue cloud and the red sequence, is primarily internally driven and dependent on mass, even if they detected a moderate acceleration of the downsizing phenomenon in overdense regions, where the rise of the quiescent population with cosmic time appears to be faster, as seen through the evolution of the transition and quenching masses, $\mathcal{M}_{\rm cross}$ and $\mathcal{M}_{\rm Q}$. Using the same dataset complemented by SDSS at low redshifts, Cooper et al. (2008) studied the connection between the star formation rate (SFR) and environment, finding hints of a reversal of that relation from $z \sim 0$, where the mean SFR decreases with local density, to $z \sim 1$, where a blue population causes an increase in the mean SFR in overdense regions; nonetheless, the decline of the global cosmic star formation history (SFH) since $z \sim 1$ seems to be caused by a gradual gas consumption rather than environment-dependent processes. A similar result on the reversing relationship SFR-environment was found by Elbaz et al. (2007), using GOODS data and SFR derived from UV and 24 μm emission.

Using spectroscopic data from the VVDS up to $z \sim 1.5$, Cucciati et al. (2006) found a steep colour-density relation at low-z, which appeared to fade at higher redshifts. In particular, they identified differences in colour distributions in low and high density regimes at low redshifts, whereas at high redshifts the environment was not found to affect these distributions. In their proposed scenario the processes of star formation and gas exhaustion are accelerated for more luminous objects and high density environments, leading to a shift with cosmic time in star formation activity toward fainter galaxies and low density environments. Scodeggio et al. (2009) studied the stellar mass and colour segregations in the VVDS at redshifts $z = 0.2{-}1.4$, using a density field computed on scales of $\sim$8 Mpc; they found that the colour-density relation is a mirror of the stellar mass segregation, that in turn is a consequence of the dark matter halo mass segregation predicted by hierarchical models.

The effects of environment on both local galaxy properties and their evolution are still uncertain, keeping the nature versus nurture debate open. From the aforementioned results, there seems to be some hint that the galaxy evolutionary path from the blue cloud to the red sequence depends on environment, but the determination of the mechanism behind this transformation, its probability of occurring, its link to both the environment and intrinsic galaxy properties is a difficult task. Different physical processes of galaxy transformation differ in terms of timescales, efficiency and observational repercussions, such as colour and morphology. The GSMF is a very suitable tool for investigating this problem and witnessing the buildup of galaxies and its dependence on environment.

In this paper, we focus on the effect of environment on field galaxies using data from COSMOS (Cosmic Evolution Survey) and zCOSMOS; in this field the most extreme overdense regions such as cluster cores are almost absent. Parallel and complementary analyses are presented in Pozzetti et al. (2010), Zucca et al. (2009), Iovino et al. (2010), Cucciati et al. (2010), Tasca et al. (2009), Kovač et al. (2010b), Vergani et al. (2010), Moresco et al. (2010), and Peng et al. (2010). The plan of this paper is the following: in Sect. 2, we describe the spectroscopic and

photometric datasets and the derived properties we used to characterise different galaxy populations; in Sect. 3 we derive the GSMFs and in Sect. 4 we analyse the different contribution of galaxy types to the GSMF in different environments. We compare our results with similar analyses in the literature and we discuss the implications for the picture of galaxy evolution in Sect. 5.

Throughout the paper we adopted the cosmological parameters $\Omega_m = 0.25$, $\Omega_\Lambda = 0.75$, $h_{70} = H_0/(70\,\mathrm{km\,s^{-1}\,Mpc^{-1}})$, magnitudes are given in the AB system and stellar masses are computed assuming the Chabrier initial mass function (Chabrier 2003).

2. Data

The zCOSMOS survey (Lilly et al. 2007) is a redshift survey intended to measure the distances of galaxies and AGNs over the COSMOS field (Scoville et al. 2007b), the largest HST survey carried out to date with ACS (Koekemoer et al. 2007). The whole field of about 2 deg^2 was observed from radio to X-ray wavelengths by parallel projects, involving worldwide teams and observatories. The coexistence of multiwavelength observations, morphologies, and spectroscopic redshifts ensures that COSMOS provides a unique opportunity to study the evolution of galaxies in their large-scale structure context.

2.1. Spectroscopy

The spectroscopic survey zCOSMOS is currently ongoing and is subdivided into two different parts: the "bright" survey, which targets ~20 000 galaxies, with a pure flux-limited selection corresponding to $15 \le I_{AB} \le 22.5$, and the "deep" survey, whose goal is the measurement of redshifts in the range $1.4 \le z \le 3.0$, within the central 1 deg^2.

The data used in this paper belong to the so-called 10 k sample (Lilly et al. 2009), consisting of the first 10 644 observed objects of the "bright" survey, over an area of 1.402 deg^2 with a mean sampling rate of ~33%. The final design of the survey aims to reach a sampling rate of ~60−70%, achieved by means of an eight-pass strategy. The observations have been carried out with VIMOS@VLT with the red grism at medium resolution $R \sim 600$. The data have been reduced with VIPGI (Scodeggio et al. 2005) and spectroscopic redshifts have been visually determined after a first hint provided by EZ (Garilli et al. 2010)[1]. The confidence on the redshift measurements has been represented by means of a flag ranging from 4, for redshifts assigned without doubts, to 0, for undetermined redshifts; a subsample of duplicated spectroscopic observations allowed us to estimate the rate of confirmation of redshift measurements, being in the range 99.8−70% depending on the flag (see Lilly et al. 2009, for details). All the redshifts have been checked by at least two astronomers. A decimal digit specifies whether the redshift is in agreement with photometric redshifts (Feldmann et al. 2006) computed from optical and near-infrared (NIR) photometry using the code ZEBRA (Zurich Extragalactic Bayesian Redshift Analyzer, Feldmann et al. 2008). For some objects, the measure resulted to be hampered by technical reasons (for instance the spectrum at the edge of the slit); in those cases, a flag −99 has been assigned. Different flags have been assigned to identify broad-line AGNs and targets observed by chance in slits.

[1] Both VIPGI and EZ are public softwares retrievable from http://cosmos.iasf-milano.inaf.it/pandora/.

2.2. Photometry

The photometry used in the following is part of the COSMOS observations and encompasses optical to NIR wavelengths: $u*$ and K_s from CFHT, B_J, V_J, g^+, r^+, i^+, and z^+ from Subaru, and Spitzer IRAC magnitudes at 3.6, 4.5, 5.8 μm. Details of photometric observations and data reduction are given in Capak et al. (2007b) and McCracken et al. (2010). The scantiness of standard stars in the photometric observations and the uncertainty in the knowledge of the filter responses result in an uncertain calibration of zero-points. To avoid this inconvenience, we optimised the photometry by applying offsets to the observed magnitudes: we computed these photometric shifts for each band minimising the differences between observed magnitudes and reference ones computed from a set of spectral energy distributions (hereafter SEDs). We adopted an approach similar to Capak et al. (2007b, see their Table 13), but considering the same set of SEDs we used to compute stellar masses detailed in Sect. 2.3, obtaining in general very similar offsets for all the filters.

2.3. Stellar masses

Stellar masses were evaluated by means of a SED fitting technique, using the code *Hyperzmass*, a modified version of the photometric redshift code *Hyperz* (Bolzonella et al. 2000). Marchesini et al. (2009) analysed the effect of random and systematic uncertainties in the stellar mass estimates on the GSMF, considering the influence of metallicity, extinction law, stellar population synthesis model, and initial mass function (IMF). On the other hand, Conroy et al. (2009) analysed the impact of the choice of the reference SEDs on the output parameters of the stellar population synthesis. Here we describe the approach and the tests we performed on our data.

We used different libraries of SEDs, derived from different models of stellar population synthesis: (1) the well-known Bruzual & Charlot (2003, hereafter BC03) library; (2) Maraston (2005, hereafter M05) and (3) Charlot & Bruzual (2010, in prep., hereafter CB07). The main difference between the three libraries is the treatment of thermally pulsing asymptotic giant branch (TP-AGB) stars. M05 models include the TP-AGB phase, calibrated with local stellar populations. This stellar phase is the dominant source of bolometric and NIR energy for a simple stellar population in the age range 0.2 to 2 Gyr. Summing up the effects of both overshooting and TP-AGB, the M05 models are brighter and redder than the BC03 models for ages between ~0.2 and ~2 Gyr (Maraston et al. 2006). The use of the M05 models leads to the derivation of lower ages and stellar masses for galaxies in which the TP-AGB stars are contributing significantly to the observed SED (i.e., ages of the order of ~1 Gyr). At older ages, the M05 models are instead bluer. CB07 is the first release of the new version of the Charlot & Bruzual library, which is not yet public. CB07 models include the prescription of Marigo & Girardi (2007) for the TP-AGB evolution of low and intermediate-mass stars. As for the M05 models, this assumption produces significantly redder NIR colors, hence younger ages and lower masses for young and intermediate-age stellar populations. A brief description of the effect on GSMFs of different choices of template SEDs can be found in the companion paper by Pozzetti et al. (2010).

All the considered libraries provide a simple stellar population (SSP) and its evolution in many age steps for a fixed metallicity and a given IMF; it is possible from the SSP models to derive the composite stellar populations that can reproduce the different types of observed galaxies, imposing a star

formation history (SFH). We compiled 10 exponentially declining SFHs with e-folding times ranging from 0.1 to 30 Gyr plus a model with constant star formation. Smooth SFHs are a simplistic representation of the complex SFHs galaxies have experienced. In Pozzetti et al. (2007), using VVDS data, we also computed stellar masses using SEDs with random secondary bursts superimposed on smooth SFHs, finding average differences well within the statistical uncertainties for most of the sample. However, repeating the comparison with the zCOSMOS 10 k sample, we estimated that about 15% of the sample has $\log \mathcal{M}_{\rm complex}/\mathcal{M}_{\rm smooth} \gtrsim 0.35$ dex (see also Pozzetti et al. 2010). Most of these galaxies are characterised by a significant fraction of stellar mass (∼5−15%) produced in a secondary burst in the past Gyr and an age of the underlying smoothly evolving population a few Gyr older than the age obtained by fitting SEDs with only smooth SFHs. We verified that these differences in the stellar mass estimate produce negligible effects on the final GSMF and therefore the results are not affected by the choice of the SEDs.

The IMF is another important parameter: different choices on the IMF produce different estimates of stellar mass, but these differences can be statistically recovered. The most widely used IMFs are those of Salpeter (Salpeter 1955), Kroupa (Kroupa 2001), and Chabrier (Chabrier 2003). The statistical differences in stellar masses are given by $\log \mathcal{M}_{\rm Salp} \simeq \log \mathcal{M}_{\rm Chab} + 0.23$ and $\log \mathcal{M}_{\rm Chab} \simeq \log \mathcal{M}_{\rm Krou} - 0.04$. Using the zCOSMOS and a mock photometric catalogue, we checked how the other parameters of the SED fitting, i.e. the age and the amount of reddening, vary when the SEDs are compiled using Chabrier and Salpeter IMFs: we found that these parameters are very similar for the two best-fit SEDs, with negligible offset and very small dispersion. In the following, stellar masses are computed assuming the Chabrier IMF.

In stellar population synthesis models, the metallicity can either evolve with time or remain fixed. In BC03, the included software does not allow us to build SEDs with evolving metallicity, although 6 different values of Z are available. To evaluate the effect of metallicity on stellar masses and GSMFs, we verified in simulated and real catalogues that the inclusion of different values of Z does not introduce a significant bias, the differences on the best-fit stellar masses being $\lesssim$0.1 dex. Using the available values of Z does not lead to a substantial improvement in the quality of the best-fits, at the cost of the introduction of an additional parameter. We therefore adopted a fixed and solar metallicity.

Dust extinction was modelled using the Calzetti's law (Calzetti et al. 2000), with values ranging from 0 to 3 mag of extinction in V band.

The χ^2 minimisation comparing observed and template fluxes at a fixed redshift $z = z_{\rm spec}$ provides the best-fit SED, with which are associated a number of physical parameters, such as age, reddening, instantaneous star formation, and stellar mass. We note that the meaning of stellar mass throughout this paper is not the integral of the star formation, because from that value we would have to exclude the return fraction, i.e., the fraction of gas processed by stars and returned to the interstellar medium during their evolution.

Tests on simulated catalogues considering the effect on stellar mass estimates of different choices of reddening law, SFHs, metallicities, and SED libraries show a typical dispersion of the order of $\sigma_{\log \mathcal{M}} \simeq 0.20$. Even a simpler technique such as that used by Maier et al. (2009) and derived from Eq. (1) of Lin et al. (2007), produces a scatter not larger than ∼0.16 dex, although with some slight trend as a function of stellar mass and redshift. These tests show that stellar mass is a rather stable parameter in SED fitting when dealing with a set of data spanning a wide wavelength range extending to NIR.

Since the fluxes provided by the available libraries at IR wavelengths have been extrapolated, the choice of filters used in determining best-fit solutions is limited to 2.5 μm rest-frame for M05 models (at longer wavelengths, these models use the Rayleigh-Jeans tail extrapolation) and to 5 μm rest-frame for BC03 and CB07 models, since at longer wavelengths the dust re-emission can contribute to the flux budget.

A problem arising when dealing with a very large number of template SEDs is to avoid non-physical best-fits. We applied two priors (the same used in Pozzetti et al. 2007, and proposed by Fontana et al. 2004 and Kauffmann et al. 2003) to avoid such a problem. In particular, we excluded best-fit SEDs not fulfilling the following requirements: (1) $A_V \leq 0.6$ if age/$\tau \geq 4$ (i.e., old galaxies must have a moderate dust extinction); (2) star formation must start at $z > 1$ if $\tau < 0.6$ Gyr (to obtain a better estimate of the ages of early-type galaxies typically fitted by these low-τ models). Moreover, we tested by means of simulations that imposing a minimum best fit age of 0.09 Gyr reduces potential degeneracies and improves the reliability of the stellar mass estimate. The maximum allowed age is the age of the Universe at $z_{\rm spec}$.

As mentioned in Sect. 2.2, the first SED fitting run over the brightest galaxies and most secure galaxy redshifts has been performed to compute the photometric offsets. We checked that additional iterations of the SED fitting and offset estimation do not significantly improve the χ^2 statistics.

To ease the comparison with literature results, in the following we present GSMFs obtained adopting the BC03 stellar masses. However, the qualitative trends are the same for any choice of stellar population synthesis model.

2.4. Environment

The density field was derived for the 10 k spectroscopic sample using different estimators combined with the ZADE (Zurich Adaptive Density Estimator, Kovač et al. 2010a) algorithm. Some of the existing studies rely heavily on photometric redshifts and projected densities computed in wide redshift slices, possibly diluting the signal from overdense regions. Cooper et al. (2005) found that photometric redshifts with accuracies of $\sigma_z \gtrsim 0.02$ hamper the computation of the density field on small scales. An important added value of COSMOS is the availability of spectroscopic redshifts obtained with a good sampling rate, making feasible an accurate estimate of the environment, with high resolution also on the radial direction.

To this aim, we used spectroscopic redshifts to delineate a skeleton of galaxy structures, and we incorporated a statistical treatment of the likelihood function of photometric redshifts computed with ZEBRA. This approach allows us to probe a wide range of environments, thanks to the precision of spectroscopic redshifts, and to reduce the Poisson noise, thanks to the inclusion of fractional contributions belonging to objects with photometric redshifts, estimated from their probability function. Results have been extensively and carefully tested on mock catalogues from the Millennium simulation (Kitzbichler & White 2007). The reconstruction of overdensities $1+\delta$ has been explored using different tracer galaxies, different spatial filters, and different weights (e.g., luminosity or stellar mass) assigned to each galaxy. The density contrast δ is defined as $(\rho - \bar{\rho})/\bar{\rho}$, where ρ is the density as a function of RA, Dec, and z and $\bar{\rho}$ is the mean density measured at the same redshift. In principle, a fully realistic physical

representation of the environment should involve the mass of the dark matter haloes in which the galaxies are embedded. This mass is clearly not directly accessible to observations, hence an affordable surrogate to weight the number density field is given by the stellar masses of the surrounding galaxies. This is a proxy of the overall density field, since galaxies are biased tracers of the underlying matter distribution. The choice of a fixed selection band results in different populations preferentially sampled at different redshifts, weighting with stellar mass should also mitigate this issue. As expected, mass-weighted overdensities have an increased dynamical range, in particular at the highest densities. As we see in Sect. 3.5, this procedure, although physically motivated, can introduce some spurious signal, mainly induced by the mass of the galaxy around which the overdensity is computed.

Another estimate of the high density environments in which galaxies reside can be obtained by selecting optical groups, as described in Knobel et al. (2009), or X-ray ones (Finoguenov et al. 2007; Finoguenov et al. 2010, in prep.); low density environments can be tracked by isolated galaxies defined using their Voronoi volumes, as in Iovino et al. (2010). The two determinations of the environment are in fairly good agreement, considering the differences of the involved scales, with most galaxies being members of groups residing in the most overdense regions (see also Sect. 3.4.2).

In the following, we use as reference the 5th nearest neighbour estimator (hereafter 5NN) of the density field, which represents a good compromise between the smallest accessible scales and the reliability of the overdensity values. In this approach, tracer galaxies, selected to be brighter than absolute magnitudes $M_B = -20.5 - z$ or $M_B = -19.3 - z$, are considered within an interval $\pm 1000\,\mathrm{km\,s^{-1}}$ centred on the central galaxy and counted, after distance sorting, until their number becomes larger than 5, considering also the fractional contribution from objects with photometric redshifts. Photometric redshifts are not crucial to the estimate of the density field, but they mainly contribute to reduce the Poisson noise and improve the agreement with the "true" density field, as has been proven by testing the method on simulated samples. Overdensities are then computed at the position of each galaxy in the spectroscopic sample, considering also the contribution to the number or mass density of the galaxy itself. We checked that the same qualitative trends of the GSMFs analysed in the following are present also when considering other estimators.

2.5. Galaxy type classification

Galaxy types can be classified in a multitude of ways, using their rest-frame colours, their SEDs, their spectroscopic features, their structural parameters and their morphologies, all of them derivable with different methods. Different classifications map different physical properties. For instance, the rest-frame colour $U-B$ and the galaxy SED are used as a proxy of the star formation activity and history, the morphology is an indicator of the dynamical state, and the two are partially independent (Mignoli et al. 2009).

Even if COSMOS offers a wide range of methods to group galaxies, we chose to use only two types of classification: photometric and morphological.

The photometric type is defined by SED fitting to the optical magnitudes, assuming as reference the same templates used by Ilbert et al. (2006): the four locally observed CWW (Coleman et al. 1980) and two starburst SEDs from Kinney et al. (1996), extrapolated at UV and mid-IR wavelengths. These six templates are then interpolated to obtain 62 SEDs and optimised with VVDS spectroscopic data. The SED fitting, a χ^2 minimisation performed with the code ALF (Ilbert et al. 2005; Zucca et al. 2006, 2009), provides as output the best-fit solution. Galaxies are then classified into two types, closely corresponding to colours of ellipticals up to early spirals (type 1, hereafter T1) and later types up to irregular and starburst galaxies (type 2, hereafter T2) to explore in a simple way the evolution of the early- and late-type bimodality.

We adopted the morphological classification presented in Scarlata et al. (2007): the availability of deep F814-band HST ACS images over the whole COSMOS field (Koekemoer et al. 2007) allows a good determination of the structural parameters on which the morphology derived with the software ZEST (Zurich Estimator of Structural Types, Scarlata et al. 2007) is based. The method is a PCA analysis using estimates of asymmetry, concentration, Gini coefficient, M_{20} (the second order moment of the 20% brightest pixels), and ellipticity. The morphological classes are the following: early-type (type 1), disk (type 2, with an associated sub-classification ranging from 0 to 3 representing the "bulgeness", derived from the n Sérsic indices, Sargent et al. 2007), and irregular galaxies (type 3). Adopting the same line of reasoning used for the photometric types, we grouped morphologically classified galaxies into two broad classes, with early-type including classes 1 and 2.0, i.e., ellipticals and bulge-dominated galaxies.

3. Mass functions

3.1. The sample

Not all the spectroscopic redshifts have the same level of reliability, as explained in Sect. 2.1. The sample we used includes only the galaxies with flags corresponding to most secure redshifts, i.e., starting from flag =1 in case of agreement with photometric redshifts. In detail, we excluded from our sample broad line AGNs (~1.8% of the statistical sample), stars (~5.9%), objects with fewer than five detected magnitudes available to compute the SED fitting (~1.7%) and objects for which the ground photometry can be affected by blending of more sources, as derived from the number of ACS sources brighter than $I = 22.5$ within $0.6''$ (~0.5%). The final sample contains 8450 galaxies with redshifts between 0.01 and 2 and 7936 in the redshift range where the following analysis is carried out, $z = 0.1-1$. For this sample, the global reliability of spectroscopic redshifts is 96%, as estimated from the mix of flags and the associated verification rates reported in Lilly et al. (2009).

3.2. Statistical weights

We took into account that the observed galaxies are only a fraction of the total number of possible available targets with the same properties by applying statistical weights to each observed object (Zucca et al. 1994; Ilbert et al. 2005). We computed the weight w_i for each galaxy in our sample as the product of two factors connected to the target sampling rate (TSR) and to the spectroscopic success rate (SSR). Here we outline the basic principles on which the computation is based, referring the reader to Zucca et al. (2009) for further details.

The TSR is the fraction of sources observed in the spectroscopic survey compared to the total number of objects in the parent photometric catalogue from which they are randomly extracted. In the case of zCOSMOS, the VMMPS tool for mask preparation (Bottini et al. 2005) has been set in such a way that

the objects have been randomly selected without any bias. A different treatment has been granted to compulsory targets, i.e., objects with forced slit positioning: they have a much higher TSR (~87%) than the "random" sample (~36%). The associated weight is $w_i^{\rm TSR} = 1/{\rm TSR}$.

The SSR represents the fraction of observed sources with a successfully measured redshift: it is a function of apparent magnitude, being linked to the signal-to-noise ratio of the spectrum, and it ranges from 97.5% to 82% for the brightest and faintest galaxies, respectively. The weight derived from the SSR is $w_i^{\rm SSR} = 1/{\rm SSR}$.

The SSR is not only a function of magnitude, but also of redshift, since the spectral features on which the redshift measurement relies can enter or go out of the observed wavelength window (Lilly et al. 2007). Therefore, the redshift distribution of the measured redshifts can be different from the real one; it is possible to take into account our lack of knowledge of the failed measurements by using photometric redshifts. Hence, we used the Ilbert et al. (2009) release of $z_{\rm phot}$ and computed the SSR in $\Delta z = 0.2$ redshift bins. We had also to consider that the characteristic emission or absorption lines are different for different galaxy types, as shown in Lilly et al. (2009). We computed the SSR in each redshift bin by separating red and blue galaxies, selected on the basis of their rest-frame $U-V$ colour. The so-called secondary targets, i.e., objects in the parent catalogue, imaged in the slit by chance, were considered separately: they are characterised by a lower SSR because they are often located at the spectrum edge or observed only at their outskirts. We computed and assigned the final weights $w_i = w_i^{\rm TSR} \times w_i^{\rm SSR}$ considering all the described dependencies.

3.3. Mass function methods

To compute the GSMFs, we adopted the usual non-parametric method $1/V_{\rm max}$ (Avni & Bahcall 1980), from which we derived the best-fit Schechter function (Schechter 1976). The observability limits inside each redshift bin, $z_{\rm min}$ and $z_{\rm max}$, were computed for each galaxy from its best-fit SED.

As in Pozzetti et al. (2010), we estimated the parametric fit of the GSMFs with both a single Schechter function, as in most published results, and the sum of two Schechter functions, which appears to provide a more accurate fit to the data at least in the lowest redshift bins. We adopted the formalism introduced by Baldry et al. (2004, 2006) using a single $\mathcal{M}^*$ to limit the number of free parameters

$$\phi(\mathcal{M}){\rm d}\mathcal{M} = \phi_1^* \left(\frac{\mathcal{M}}{\mathcal{M}^*}\right)^{\alpha_1} \exp\left(-\frac{\mathcal{M}}{\mathcal{M}^*}\right) {\rm d}\frac{\mathcal{M}}{\mathcal{M}^*} + \phi_2^* \left(\frac{\mathcal{M}}{\mathcal{M}^*}\right)^{\alpha_2} \exp\left(-\frac{\mathcal{M}}{\mathcal{M}^*}\right) {\rm d}\frac{\mathcal{M}}{\mathcal{M}^*}. \quad (1)$$

Until now the need to model a faint-end upturn has been studied in luminosity function (LF) studies, both in the field (Zucca et al. 1997; Blanton et al. 2005b) and in clusters and groups (Trentham 1998; Trentham et al. 2005; Popesso et al. 2007; Jenkins et al. 2007). The departure of the GSMF from a single Schechter function at low stellar masses was noticed by Baldry et al. (2006, 2008) and Panter et al. (2004) for SDSS data. At higher redshifts, an a posteriori look at the published GSMFs often reveals such an upturn.

We refer to $\mathcal{M}_{\rm min}$ as the lowest mass at which the GSMF can be considered reliable and unaffected by incompleteness on $\mathcal{M}/L$ (see Ilbert et al. 2004; Pozzetti et al. 2007). A complete description of the procedure can be found in Pozzetti et al. (2010). Our aim is to recover the stellar mass up to which all the galaxy types contributing significantly to the GSMF can be observed. We derived this value in small redshift slices by considering the 20% faintest galaxies, i.e., those contributing to the low-mass end of the GSMF. For each galaxy of this subsample, we computed the "limiting mass", that is the stellar mass that the object would have had at the limiting magnitude of the survey, $\log \mathcal{M}_{\rm lim} = \log \mathcal{M} + 0.4(I - 22.5)$. For each redshift bin, we define as minimum mass the value corresponding to 95% of the distribution of limiting masses and we smooth the $\mathcal{M}_{\rm min}$ versus z relation by means of an interpolation with a parabolic curve. The minimum stellar mass we adopt is the value up to which we can reliably compute the GSMF in each considered redshift bin, i.e. the $\mathcal{M}_{\rm min}$ at the lowest extreme of the interval, since the $1/V_{\rm max}$ method corrects the residual volume incompleteness.

We note that this limit substantially decreases the number of objects considered in each redshift bin to derive the GSMF. The redshift intervals [0.10, 0.35], [0.35, 0.50], [0.50, 0.70], and [0.70, 1.00] were chosen to contain a similar number of galaxies and the values we obtained for the limiting mass of the total sample are $\log \mathcal{M}_{\rm lim}/\mathcal{M}_\odot = 8.2, 9.4, 9.9, 10.5$ from the lowest to the highest redshift bin. When dealing with GSMFs divided into galaxy types, the minimum masses are obtained separately for each subsample.

3.4. The choice of the environment definition

As mentioned in Sect. 2.4, the density field of the COSMOS field (see Kovač et al. 2010a) was reconstructed for different choices of filters (of fixed comoving aperture or adaptive with a fixed number of neighbours), tracers (from flux-limited or volume-limited subsamples), and weights (stellar mass, luminosity or no weight, i.e., considering only the number of galaxies).

We tested the options that allow an unbiased comparison over the whole redshift range, from $z = 0.1$ to 1.0. In particular, we explored the 5NN estimator and the 5NN mass-weighted one (hereafter 5NNM), both of them computed using volume-limited tracers, with two choices of luminosity limits: $M_B \leq -20.5 - z$ (bright tracers) and $M_B \leq -19.3 - z$ (faint tracers), where M_B is the absolute magnitude in the B band computed with ZEBRA. The absolute magnitude cut was derived by considering the distribution of absolute magnitudes versus redshift, the so-called Spaenhauer diagram (Spaenhauer 1978), and the evolution of the parameter M_B^* of the LFs (Zucca et al. 2009). Two different limits are necessary because of the rareness of bright tracers at low redshift and the incompleteness of faint tracers at high redshift; for this reason, the two overdensity estimates cannot be computed over the whole redshift range, but only at [0.1, 0.7] and $z = [0.4, 1.0]$ for faint and bright tracers, respectively.

3.4.1. The effect of environment tracers on GSMF

Two problems affect the study on the evolution of GSMFs as a function of environment, which must be solved: (1) we have to understand whether the 5NNM estimator is a more robust tracer of the environment, as predicted theoretically; (2) we have to be certain that the use of two different tracers, e.g., with a change at $z = 0.7$, does not introduce a spurious signal that may be misinterpreted as an evolutionary trend.

To answer both questions, we used as a test case the redshift interval [0.4, 0.7], where all the estimates are available, and we computed the quartiles of the $1 + \delta$ distribution in this redshift bin considering only the objects with masses higher than

the minimum mass. Henceforth, we refer to the lowest and highest quartiles of $1+\delta$ as D1 and D4, respectively. In the reminder of the paper, we focus our study on these two extremes.

In Fig. 1, panel (a), we compare the GSMFs derived using a single Schechter function fit, for 5NN and 5NNM overdensity estimators, both using the faint volume-limited tracers. The separation of GSMFs between D1 and D4 environments is more prominent when considering the mass-weighted estimator, because of the larger dynamical range of the $1+\delta$ values studied. In particular, the main difference is in the massive part of D1 GSMF: massive galaxies in low density environments using 5NN move to intermediate densities for 5NNM estimator because of their high stellar masses. This decreases the number (and therefore the normalisation of the GSMF) of massive galaxies in low density environments when the 5NNM estimator is adopted. To test whether this enhancement of the difference between the D1 and D4 GSMFs is real, we performed the following test: we removed as much as we could the mass-density relation by shuffling the original catalogue and computing overdensities considering objects with their original coordinates, but assigning to each one the observed properties (magnitudes, stellar mass, weight) of the 25th following object after redshift sorting. Both 5NN and 5NNM overdensities and their quartiles were then recomputed, since the shuffling also changes the tracers. The choice of the 25 object jump is a compromise between the requirements of preserving a similar probability of being observed at the chosen redshift (i.e., avoiding unphysical galaxy properties if a large jump in redshift is allowed) and selecting objects possibly not in the same structure, where we know galaxies share similar properties (in this case the mass-density relation would not be removed). In this test, we expect that GSMFs derived in D1 and D4, regardless of the estimator of the density contrast used, to be approximately the same, since, after reshuffling, massive galaxies should no longer occupy preferentially high density environments. Moreover, we also expect that the 5NN and 5NNM estimators of the density should produce similar results, since the 5 neighbours should have a random distribution of their stellar masses. The comparison between GSMFs with 5NN and 5NNM "shuffled" overdensities is shown in Fig. 1, panel (b). For 5NN, we see that GSMFs in D1 and D4 are more similar than before, but not coincident; this may be due to an insufficiently large amount of shuffling being used to separate masses and environment in the biggest structures. Furthermore, the 5NN and 5NNM estimates are still quite different, mainly at the high masses in D4. These results may be caused by the non-negligible influence of the stellar mass of the object itself in the case of the 5NNM estimator, possibly enhanced by a residual signal in the mass-density relation.

In our last test to interpret this residual signal, we removed the central galaxy when computing $1+\delta$ from the original catalogue: the comparison of the resulting GSMFs is in Fig. 1 panel (c), which shows now fully consistent GSMFs at high and low densities as defined from 5NN and 5NNM estimators.

These tests seem to indicate that the mass weighting scheme assigns too great an importance to stellar masses on scales of the order of the galaxy itself. Thus, we attempted to avoid any possible bias due to stellar mass over-weighting, despite its physically motivated link with the halo mass, by discarding the 5NNM estimator and we performed our analysis using number-weighted overdensities.

To help resolve the second problem, we tested whether the change of the tracers at $z = 0.7$ could introduce some change in the GSMF, which can be misinterpreted as evolution. We already know that the scales probed at the same $1+\delta$ are more

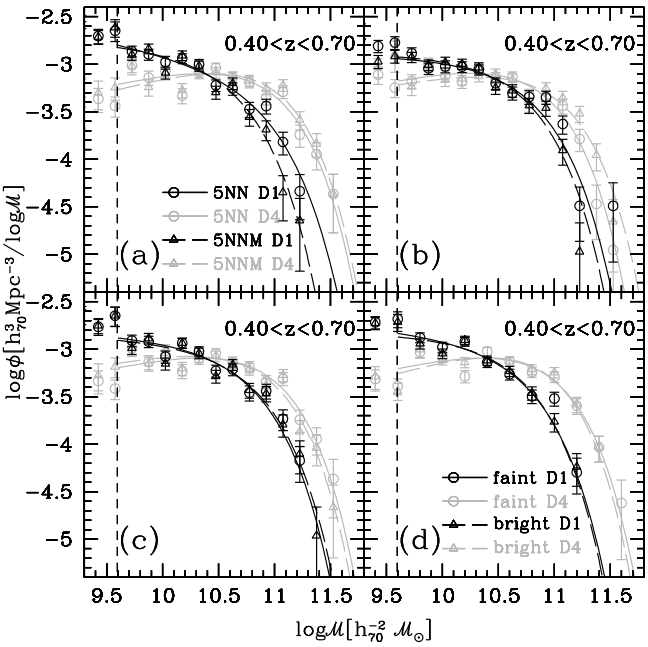

Fig. 1. a) Comparison of GSMFs for environment estimates from 5NN and 5NNM volume limited with faint tracers: Black: D1 (underdense); Grey: D4 (overdense). Solid line and empty dots: 5NN. Dashed line and empty triangles: 5NNM. The vertical dashed line represent the value of $\mathcal{M}_{\rm min}$ at $z = 0.4$. **b)** As in panel **a)**, but 5NN and 5NNM overdensities have been estimated after a random shuffling of galaxy properties to remove the mass-density relation. **c)** As in panel **a)**, but 5NN and 5NNM overdensities have been estimated without considering the properties of the central galaxy. **d)** GSMFs for bright ($M_B \leq -20.5 - z$, dashed lines and empty triangles) and faint ($M_B \leq -19.3 - z$, solid lines and empty dots) tracers using 5NN overdensities in the D1 (black) and D4 (grey) environments.

or less twice as large for bright than faint tracers (Kovač et al. 2010a), therefore it is not possible to use the same $1+\delta$ threshold for both faint and bright tracers. To overcome this problem, we determined the quartiles of $1+\delta$ separately for each redshift bin. The results of this test are shown in panel (d) of Fig. 1. In the $z = 0.4$–0.7 bin, where both tracers are available, the GSMFs obtained with the two tracers, with independently computed quartiles, are completely consistent with each other in under and overdense environments D1 and D4, and therefore we assume we can safely compare the results at redshifts $z < 0.7$ computed with faint tracers to those computed at $z \geq 0.7$ with the bright ones.

3.4.2. Definition of overdensity quartiles

As already mentioned, we traced the effect of extreme environments on the evolution of galaxies by considering the quartiles D1 and D4 of the $1+\delta$ distribution, using 5NN volume-limited overdensities. The quartiles were computed at each redshift bin considering only the population of galaxies more massive than the minimum stellar mass considered for the GSMF (see Sect. 3.3) in the highest redshift bin, i.e., $\log \mathcal{M}_{\rm min}/\mathcal{M}_\odot \simeq 10.5$, to ensure that this definition is unaffected by the variation as a function of redshift in the observable mass range, populated by different mix of galaxy types. The quartile definition used throughout this paper is shown in Fig. 2. The median scales probed by the 5th nearest neighbour range from 0.87 Mpc h_{70}^{-1}

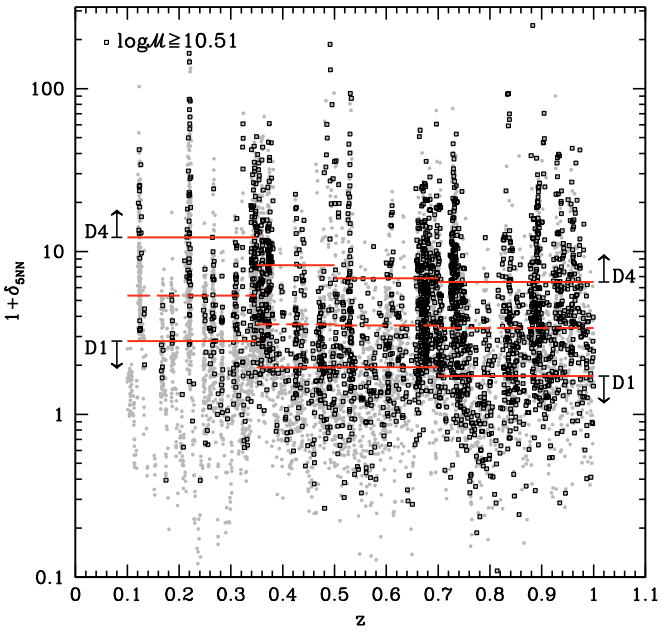

Fig. 2. Definition of quartiles for the 5NN estimator using volume-limited tracers: grey points represent the full sample, black squares the galaxies with masses above the $\mathcal{M}_{\rm min}$ computed in the last redshift bin, horizontal segments show the values of the quartiles of $1+\delta$ computed from the distribution of these massive galaxies, and the dashed ones indicate the median.

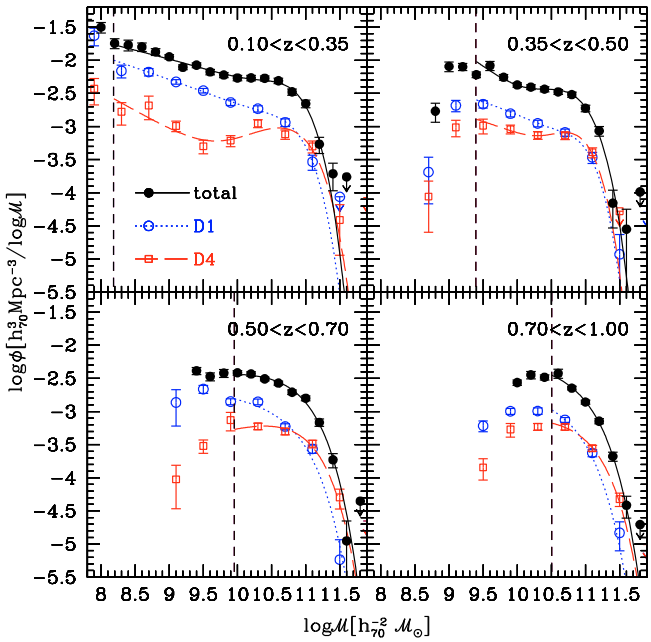

Fig. 3. The MFs in the extreme quartiles D1 and D4 of the 5NN volume-limited overdensities. Black: total GSMF, with $1/V_{\rm max}$ dots and their Poissonian error bars and Schechter function fit (double Schechter function in the first two redshift ranges and a single one at higher redshifts). Blue: lowest $1+\delta$ quartile. Red: highest density quartile.

in the D4 environment at low redshift to 7.57 Mpc h_{70}^{-1} in the D1 quartile at the highest redshift bin, where we have to use bright tracers.

The trend toward higher values of overdensity at lower redshifts is in some measure expected from the growth of structures, which amplifies the dynamic range of overdensities, but this increase cannot be quantified using the linear approximation, which is invalid on the scales probed by our density estimates. The different values of the $1+\delta$ quartiles in the different redshift bins correspond to very similar scales when the same tracers are used.

It is not easy to compare the values of density contrast in Fig. 2 with those of known objects, such as rich clusters or voids, because of the different definitions of environment and the different scales probed. A possible comparison is instead feasible with the distribution of $1+\delta$ for the members of galaxy groups identified in the same COSMOS field. This comparison is shown in Fig. 22 of Kovač et al. (2010a), where it is possible to see that galaxy members of optical groups with ≥2 members have a distribution of overdensities that peaks at $1+\delta\sim 6$, whereas richer groups and X-ray candidate clusters typically have $1+\delta\sim 20$. Although the different classifications of the environment are obviously related, they are not perfectly coincident, with ∼59% of the objects in the group catalogue used by Kovač et al. (2010b) belonging to D4 (and only 6% to D1) and ∼73% of the objects classified as "isolated" by Iovino et al. (2010) being in D1 (and only 0.2% in D4).

3.5. Mass functions in different environments

The GSMFs in the two extreme environments are shown in Fig. 3: the bimodality is clearly visible in the global GSMFs (Pozzetti et al. 2010, see also the points and lines in Fig. 3), with an upturn at the low-mass end around $\mathcal{M}\sim 10^{9.5}\,\mathcal{M}_\odot$, which is more pronounced in the high density regions, at least in the two lowest redshift bins. We used the double Schechter function fit only up to $z\sim 0.5$, where the dip in the GSMFs falls at stellar masses higher than $\mathcal{M}_{\rm min}$. Because of our choice of environment definition, the normalisation of D1 and D4 GSMFs does not have a clear physical meaning, since the volumes occupied by each galaxy are referred to the total volume of the survey and the number of galaxies in each environment is not 1/4 of the total sample. To obtain a more meaningful definition of the normalisation, we should compute the volume occupied by the structures with the considered ranges of $1+\delta$; here we compare only the GSMF shapes, hence defer a more in-depth study of the normalisation to a future analysis. A striking difference in GSMF shapes is evident, with massive galaxies preferentially residing in high density environments, characterised on average by a higher $\mathcal{M}^*$, and with a steeper slope than the D1 GSMFs at $z\geq 0.35$. The different shapes and the strong bimodality in the D4 GSMF can be interpreted in a similar way to the global one (Pozzetti et al. 2010) by the different contribution of different galaxy types, as we see in the next section. The parameters of the Schechter fits to the GSMFs are listed in Table 1.

4. Evolution of galaxy types in different environments

The need to use a double Schechter function to fit the global and environment-selected GSMFs at least up to $z\sim 0.5$ may be linked to the contribution of different galaxy populations. Galaxies with the same luminosity may be characterised by very different $\mathcal{M}/L$, which can explain why it is difficult to identify the bimodal shape of LFs, even though this bimodality was first detected in LFs.

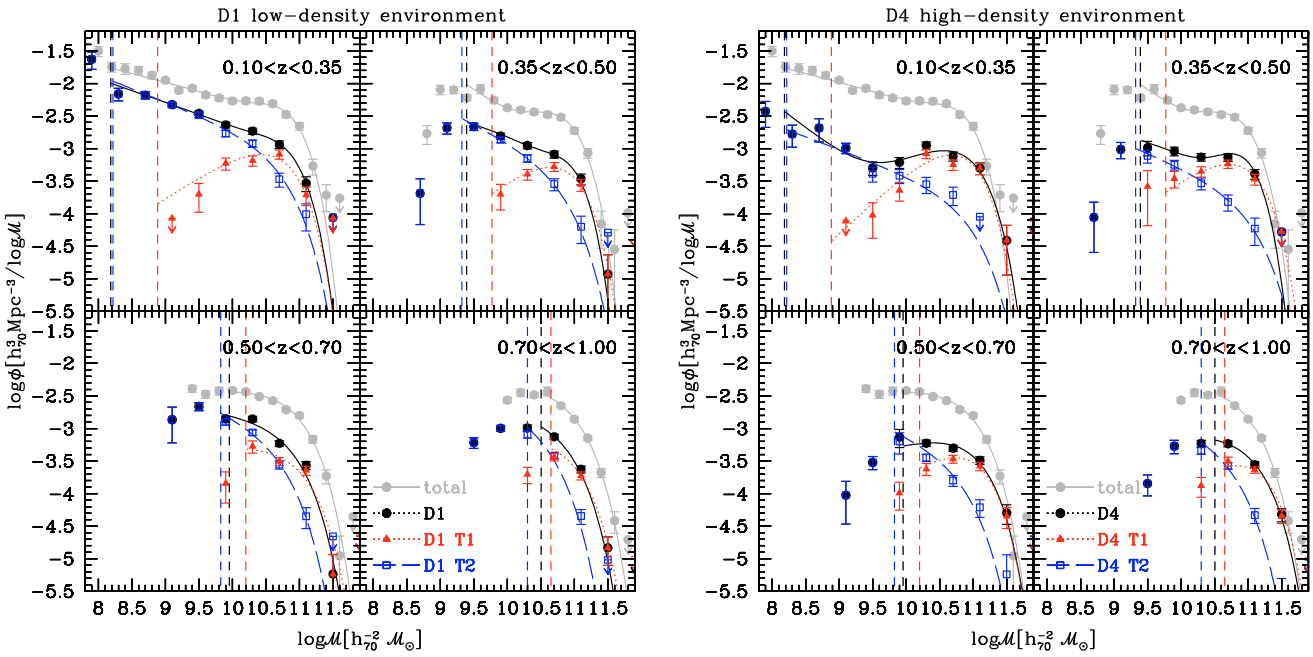

Fig. 4. *Left*: quartile D1 (low density environment). *Right*: quartile D4 (high density). Grey: total GSMF. Black: MF relative to the considered quartile. Red triangles and dotted lines: photometric early-type galaxies. Blue squares and dashed lines: photometric late-type galaxies. At high masses, the upper limit points show the 2σ confidence limits for 0 detections following Gehrels (1986).

Table 1. Parameters of the GSMF in the low and high-density environments.

	z	α_1	α_2	$\log \mathcal{M}^*/\mathcal{M}_\odot$	ϕ_1^*/ϕ_2^*
D1	0.10–0.35	−1.35	+0.14	10.53	1.61
	0.35–0.50	−1.25	+0.82	10.52	0.79
	0.50–0.70	−1.13	...	10.82	...
	0.70–1.00	−1.12	...	10.80	...
D4	0.10–0.35	−1.80	–0.33	10.76	0.01
	0.35–0.50	−1.28	+0.95	10.52	0.50
	0.50–0.70	–0.70	...	10.92	...
	0.70–1.00	–0.90	...	10.98	...

To study the contribution of galaxies with different photometric types and morphologies in the extreme environments, we computed the GSMFs of D1 and D4, defined as in Sect. 3.5, by dividing each sub-sample into galaxy classes. The values of $\mathcal{M}_{\rm min}$ were computed separately for early/elliptical/bulge-dominated and late/spiral/disc-dominated galaxies. These values differ significantly, especially at low redshift, confirming the very different distributions of $\mathcal{M}/L$.

The results for the contribution of different photometric types to D1 and D4 GSMFs are presented in Fig. 4, and the best-fit parameters of the single Schechter function fits are given in Table 2. Dividing the sample into the two broad morphological classes results in qualitatively similar GSMFs.

Looking at the plots in Fig. 4, it is clear that the stronger bimodality in the first two redshift bins in the D4 GSMF is primarily due to the larger contribution of early-type galaxies. As for the global GSMF, in both of the considered environments early-type galaxies are dominant at high masses ($\log \mathcal{M}/\mathcal{M}_\odot \gtrsim 10.7$), while their contribution rapidly decreases at intermediate masses. On the other hand, late-type galaxies, which have much steeper GSMFs, start to dominate at intermediate and low masses ($\log \mathcal{M}/\mathcal{M}_\odot \sim 10$).

Table 2. Parameters of the GSMF for the two photometric types T1 (early-type galaxies) and T2 (late-type galaxies) in the low and high-density environments.

	z	α	$\log \mathcal{M}^*/\mathcal{M}_\odot$
D1T1	0.10–0.35	$-0.33^{+0.46}_{-0.37}$	$10.60^{+0.15}_{-0.11}$
	0.35–0.50	$-0.17^{+0.71}_{-0.55}$	$10.72^{+0.32}_{-0.21}$
	0.50–0.70	$-0.90^{+0.85}_{-0.60}$	$10.93^{+0.26}_{-0.25}$
	0.70–1.00	[−0.90]	$10.88^{+0.10}_{-0.10}$
D1T2	0.10–0.35	$-1.41^{+0.11}_{-0.07}$	$10.71^{+0.18}_{-0.23}$
	0.35–0.50	$-1.51^{+0.32}_{-0.25}$	$10.81^{+0.51}_{-0.36}$
	0.50–0.70	$-1.45^{+0.52}_{-0.36}$	$10.70^{+0.28}_{-0.26}$
	0.70–1.00	[−1.45]	$10.59^{+0.06}_{-0.08}$
D4T1	0.10–0.35	$-0.03^{+0.46}_{-0.32}$	$10.68^{+0.18}_{-0.21}$
	0.35–0.50	$-0.23^{+0.59}_{-0.45}$	$10.82^{+0.22}_{-0.20}$
	0.50–0.70	$-0.28^{+0.65}_{-0.48}$	$10.87^{+0.15}_{-0.18}$
	0.70–1.00	[−0.28]	$10.97^{+0.06}_{-0.06}$
D4T2	0.10–0.35	$-1.39^{+0.13}_{-0.09}$	$10.92^{+0.32}_{-0.38}$
	0.35–0.50	$-1.43^{+0.19}_{-0.14}$	$11.02^{+0.22}_{-0.45}$
	0.50–0.70	[−1.43]	$10.81^{+0.13}_{-0.15}$
	0.70–1.00	[−1.43]	$10.75^{+0.07}_{-0.07}$

Notes. When the parameter α is undetermined, we fixed it to the best-fit value in the previous bin of the same environment. Error bars are at 1σ confidence level.

In addition to assessing the relative contributions of different galaxy types in D1 and D4, it is sensible to ask whether the shape of the GSMFs of galaxies of the same type is the same in different environments, i.e., whether a "universal" mass function of early/late-type galaxies does exist. In Fig. 5, we compare early- and late-type GSMFs in the two environments, in each redshift bin renormalised with the number density computed for

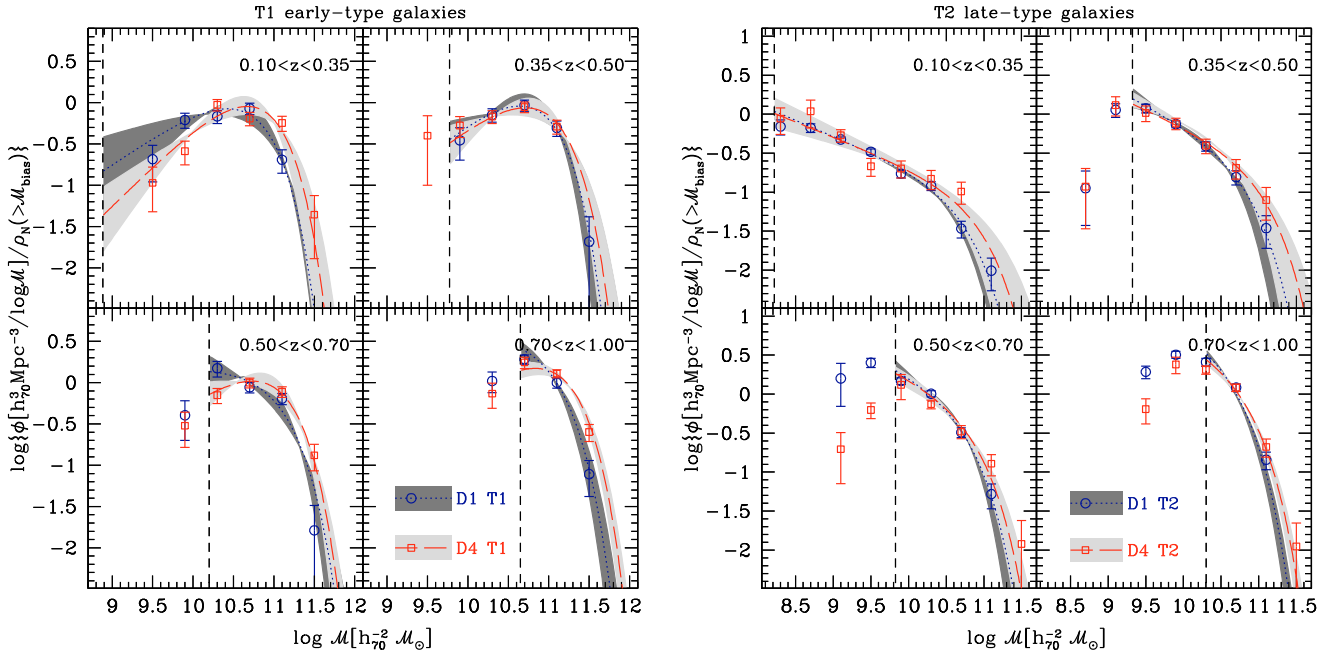

Fig. 5. *Left*: GSMFs of photometric early-type galaxies in D1 and D4 environments, renormalised to number density =1 for stellar masses $>\mathcal{M}_{\rm min}$. *Right*: the same for photometrically late type galaxies. Dotted lines, circles and dark shaded regions represent the GSMFs in underdense regions, D1. Dashed lines, squares and light shaded regions illustrate D4 GSMFs.

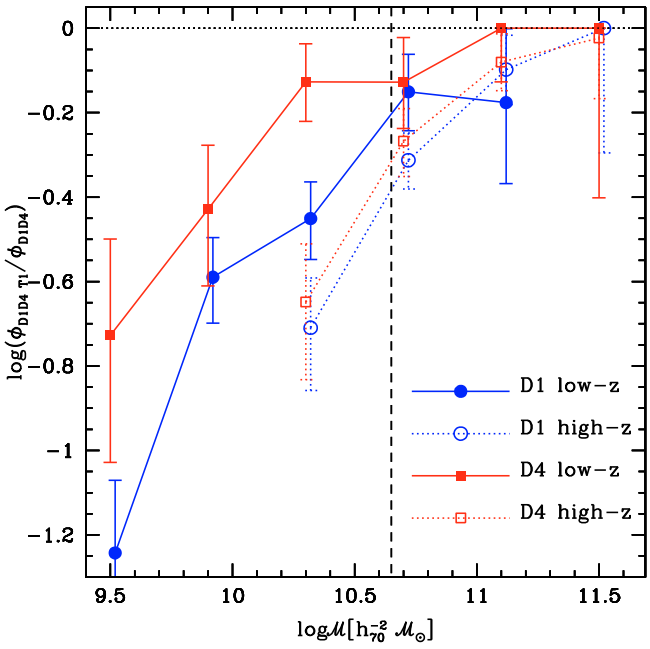

Fig. 6. Evolution of the fractional contribution of the photometric early-type to the global MFs (the late-type fractional contribution is complementary to the one shown in this plot) in the two extreme environments. Blue lines and circles refer to the low density environment D1 (displaced by 0.02 in the abscissa to avoid overlapping), red lines and squares to the high density sample D4. Dotted lines and empty symbols represent the highest redshift bin $z = [0.7, 1.0]$, solid lines and filled points the lowest one, $z = [0.1, 0.35]$. The vertical dashed line indicates $\mathcal{M}_{\rm min}$ in the high redshift bin (the value at low redshift is outside the plot). Error bars have been computed as 16−84% of the distribution of Monte Carlo simulations.

masses $\geq\mathcal{M}_{\rm min}$. The shapes of the GSMFs differ slightly, there being a slightly higher density of massive galaxies in overdense regions; however the similarity of the GSMFs in all the redshift bins, and in particular for late-type galaxies, is remarkable and somewhat unexpected. If the shape of the GSMF of galaxies of the same type is similar in different environments, any difference seen in the total GSMFs in under- and overdense regions at low redshift should be due to the different evolution of their normalisations.

To examine the differential contribution of various galaxy types in different environments, we can compute the evolution of the ratio of the GSMF of a given galaxy class to the global GSMFs in each environment. In Fig. 6, we show the ratio of $1/V_{\rm max}$ estimates of early-type GSMF in over and underdense regions for the two extreme redshift bins. The trend for late-type galaxies is the opposite of that shown in the figure. The error bars were computed using a Monte Carlo simulation considering Gaussian distribution of errors of rms derived from Poissonian error bars using $1/V_{\rm max}$ method. The 16% and 84% of the 100 000 iterations of the ratio distribution are reported in the plot as error bars. The vertical dashed line shows the value of $\mathcal{M}_{\rm min}$ for early-type galaxies in the redshift bin $z = 0.7-1.0$. Despite the large error bars, Fig. 6 illustrates that in the high redshift bin the fractional contributions of photometric early-types to the GSMF in different environments are more or less the same for D1 and D4 at all the masses we can safely study. On the other hand, the fractional contribution is significantly different at low redshift, mainly at intermediate stellar masses ($\log\mathcal{M}/\mathcal{M}_\odot \lesssim 10.5$). This trend appears to imply that there is a more rapid growth with time in high density environments of the fractional contribution of early-type galaxies. At intermediate masses, the differences between the two extreme environments are larger: high stellar masses ($\log\mathcal{M}/\mathcal{M}_\odot \gtrsim 10.7$) are populated mainly by passive red galaxies in both environments, while at lower masses ($\log\mathcal{M}/\mathcal{M}_\odot \lesssim 10$, in the low redshift bins, where it is possible to probe them) the population of late-type/star-forming galaxies dominates in all the environments.

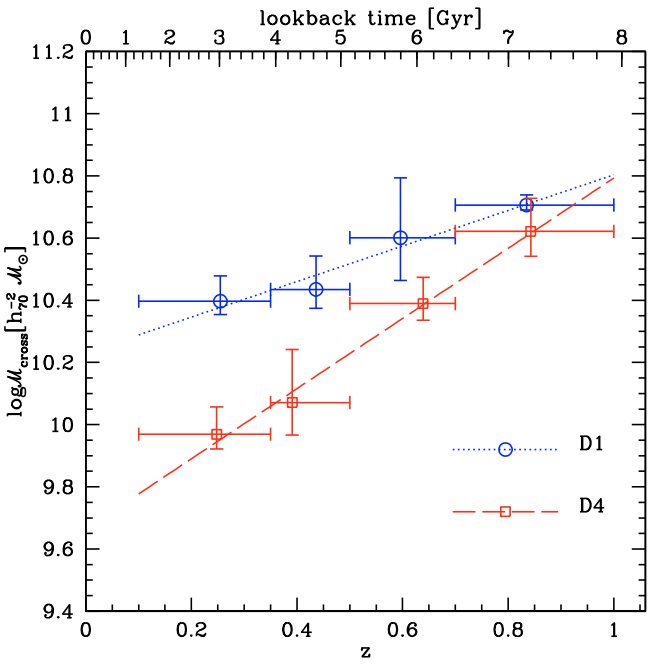

Fig. 7. $\mathcal{M}_{\rm cross}$ of photometric types in the extreme quartiles D1 and D4. Blue: low-density environments. Red: high-density. The points are located at the median redshift of the early plus late samples and error bars represent the width of the redshift bin and the error in the GSMF ratio from $1/V_{\rm max}$ method. A linear fit to the points is also shown.

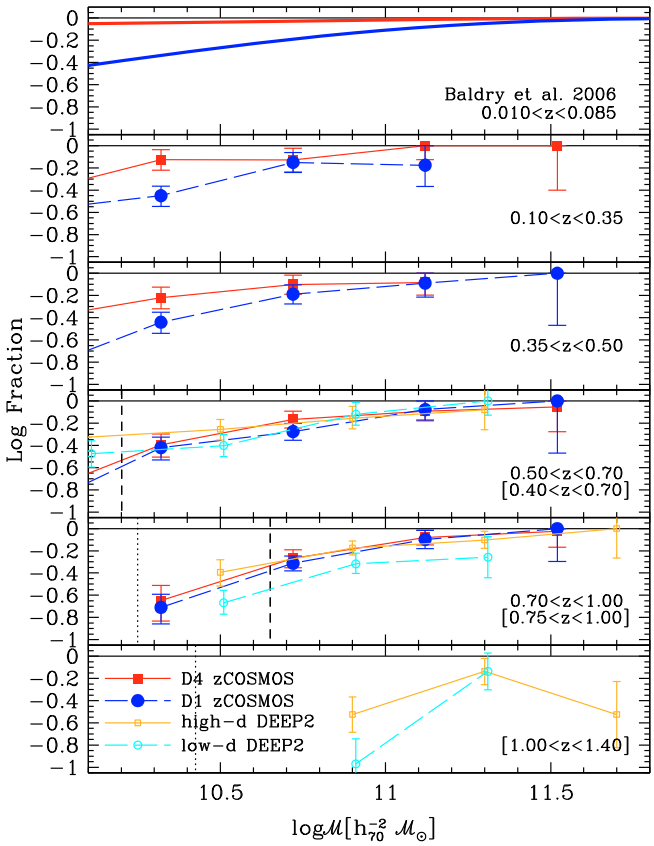

Fig. 8. Evolution of the fractional contribution of the early-type/red galaxies to the global MFs in low and high density environments from the surveys SDSS, zCOSMOS, and DEEP2. In the low redshift bin, red and blue lines are computed from Eq. (10) by Baldry et al. (2006), representing the fraction of red galaxies in the highest and lowest environmental densities in their SDSS analysis. In the other redshift bins, red solid lines and filled squares represent the zCOSMOS high-density sample D4, and blue long-dashed lines and filled circles the low-density sample D1. Orange and cyan lines and empty symbols represent the values of the analogous fractions taken from Bundy et al. (2006). The vertical dashed lines mark $\mathcal{M}_{\rm min}$ in zCOSMOS, and vertical dotted lines represent the $K_{\rm s}$-band completeness limits in Bundy et al. (2006). Redshift ranges between brackets refer to DEEP2 binning.

In a scenario that is consistent with these data, which indicate there is an increase in early-type galaxies with cosmic time, blue intermediate-mass galaxies are being transformed into more massive red galaxies, after quenching their star formation in a more efficient way in overdense than underdense regions. A possible way to quantify this difference in evolutionary speed is by analysing the evolution with redshift of $\mathcal{M}_{\rm cross}$, which represents the mass above which the GSMF is dominated by early-type galaxies. We show this quantity computed from $1/V_{\rm max}$ points in Fig. 7 for different photometric types. We can see that since $z \sim 1$, where the $\mathcal{M}_{\rm cross}$ values in low and high density environments were similar, the subsequent evolution produces a significant difference between the two $\mathcal{M}_{\rm cross}$ values. The ratio of $\mathcal{M}_{\rm cross}$ in the highest to lowest redshift bins implies an evolution of a factor ∼2 in low density and ∼4.5 in high density regions. From a different point of view, the plot in Fig. 7 indicates that the environment begins to affect the evolution of galaxies at $z \sim 1$, causing in the lowest redshift bin a delay of ∼2 Gyr in underdense relative to overdense regions before the same mix of galaxy types is observed in high density regions.

5. Discussion

5.1. Comparison with literature data

As mentioned in Sect. 1, a similar analysis of the influence of environment on the evolution of the GSMF of red and blue galaxies was carried out by Bundy et al. (2006) using DEEP2 data. They considered a sample in the redshift range $0.4 < z < 1.4$, partially overlapping with ours, and a the definition of galaxy types and environment that slightly differed; their galaxy types are defined on the basis of the rest-frame colour $U - B$ and their under- and overdense environments are defined with respect to the average local density for the majority of their analysis. Since, as the authors also state, most of the galaxies belong to regions around the average density, we do not expect to find that the environment has a significant influence of the redshift evolution of galaxies. However, they also considered the extremes of the density field in their Fig. 11, where they present the evolution with redshift in the fractional contribution of red and blue galaxies.

We compare our results obtained using our definitions of environment and galaxy types, with the Bundy et al. (2006) paper in Fig. 8. At low redshift, we plot for reference the results of Baldry et al. (2006), who used SDSS data divided into density bins and galaxy types separated by means of the colour bimodality. The lines in the plot are derived from their Eq. (10), adopting their highest and lowest density values. The results from the two high-z surveys are in reasonably good agreement. The largest difference is in low density environments in our redshift bin $z = [0.70, 1.00]$, but results are marginally consistent with each other. When we study the evolution of the mass function fractions derived from the three surveys, the main visible trend is the continuous increase with time in the fractional contribution

of red/early-type galaxies in all environments, which is an alternative way of observing the build-up of the red sequence and its increasing population at lower stellar masses. The differences between low and high density environments seem to increase towards low redshift, whereas at high redshifts the quite large error bars prevent our drawing robust conclusions, which may also depend on the particular definitions of the samples.

Cooper et al. (2010a) analysed the colour-density relation in the DEEP2 sample and claimed that the environmental dependence is still present at $z = 1$. In contrast to our analysis, they considered the top 10% of the high-density sample, using the density field computed at the distance of the 3rd-nearest neighbour in the total flux-limited sample. With this choice, they explored a smaller scale environment than the one used in the present paper. For instance, they state that the typical distance involved in the computation of their top 5% overdensities is about 35″ at $z \sim 0.9$, corresponding to a comoving scale $\sim 0.37\,h^{-1}$ Mpc. The average scale of our top 5% overdensities in our highest redshift bin is $\sim 1.1\,h^{-1}$ Mpc. Therefore, the results of the two surveys do not necessarily disagree if the environmental mechanism modifying galaxy properties at $z \gtrsim 1$ is mainly effective on small scales.

Other studies of the evolution of the GSMFs of galaxies of different types and morphologies are presented in Pozzetti et al. (2010), Ilbert et al. (2010), Bundy et al. (2010), and Drory et al. (2009), though without incorporating directly the environmental effects. They all find that the global GSMF has a bimodal shape, with the need to use two Schechter functions eventually extending to the single galaxy types GSMFs, as found by Drory et al. (2009). These authors interpret the presence of a plateau at $\sim 10^{10} \mathcal{M}_{\odot}$ in blue galaxies as a signature of either a change in star formation efficiency, which is more dramatic at lower masses, or an increase in the galaxy assembly rate at higher masses. At low redshift, the dip appears to move from blue to red galaxies, because blue massive galaxies become red and satellite galaxies undergo environmental quenching. Bundy et al. (2010), Ilbert et al. (2010), and Pozzetti et al. (2010) compare results obtained for galaxies classified from rest-frame colours and morphology, finding that the transformation from blue to red colours and from disk-dominated to bulge-dominated morphologies may be due to two or more processes, which are either environmentally driven (strangulation, major or minor merging with varying amounts of gas) or internal (instabilities, gas consumption, morphological quenching, AGN feedback) (Bundy et al. 2010). Any scenario should account for the non-negligible fraction of quiescent disk-dominated galaxies at low masses, and involve processes with different timescales for the shutdown of the star formation and the morphological transformation (e.g. Pozzetti et al. 2010), whereas for massive galaxies the correspondence of red colours and elliptical morphologies should be explained by a single dominant mechanism, probably associated with secular evolution (Oesch et al. 2010). We explore in more detail the differences between morphological and colour transformation in different environments in Sect. 5.2.

Scodeggio et al. (2009) study the rest-frame colours of VVDS galaxies at $0.2 < z < 1.4$ in environments based on the density contrast on scales of ∼8 Mpc, and conclude that the segregation of galaxy properties is ultimately the result of the large scale environment, via the mass of the dark matter halo. This conclusion agrees with our findings: from Fig. 3, we infer that the large-scale environment sets up the stellar mass distribution, which is in turn is linked to the mass of the hosting haloes, and its evolution.

At low redshift, the bimodality of the GSMF has also been detected: for instance, from the SDSS dataset, Baldry et al. (2006) and Baldry et al. (2008) detect a significant upturn at low stellar masses with respect to the single Schechter function on the global and environment dependent GSMFs.

Considering the alternative definition of environment, i.e., galaxy clusters and groups, we also find in the literature signs of an excess of low mass systems, for instance by converting the composite LF of RASS-SDSS clusters by Popesso et al. (2006) to GSMFs by making an assumption about the mass-to-light ratio, as done in Baldry et al. (2008). A steep low mass end is seen for clusters, steeper than the upturn noticed in the field from the SDSS and also, to a lesser extent, than our α_1 value in D4 in the low redshift bin. The mechanisms responsible for the bimodal nature of the GSMFs should therefore operate in both the field and high density environments, but in the most dense regions they should be able to originate the steepest low mass end. For instance, in Rudnick et al. (2009), the same bimodality in the LF can be seen for SDSS clusters at low redshifts, and in Bañados et al. (2010) for galaxies members of Abell 1689 at $z = 0.183$. Analyses of high redshift clusters (e.g. Poggianti et al. 1999, 2009; Desai et al. 2007; Sánchez-Blázquez et al. 2009; Simard et al. 2009; Patel et al. 2009a,b; Just et al. 2010; Wolf et al. 2009; Gallazzi et al. 2009; Balogh et al. 2007, 2009; Wilman et al. 2009; Treu et al. 2003) are mainly focused on the buildup of the red sequence and the evolution of the fraction of morphological types, in particular S0 galaxies, linked especially to the peculiar mechanisms acting on these densest environments.

In these quoted works, a complex picture, but broadly consistent within the uncertainties, is emerging for the evolutionary paths of galaxies, with many mechanisms playing a role, whose relative importance is a function of the mass, environment and past history of each considered system.

5.2. The mechanism and timescale of galaxy transformation

Figures 6 and 7 provide some clues about the timescale and mechanism responsible of galaxy quenching in different environments. We have found that the evolution in the high density regions is more rapid than in low density ones, i.e., the rate of transformation into photometric early-types is higher from $z = 1$ to low redshifts in overdense regions than underdense ones. Therefore, some of the mechanisms responsible for quenching the star formation, and then transforming blue galaxies into passive ones, must be environment dependent. The physical processes operating on galaxies and transforming their colours and/or morphologies can be internally or externally driven and gravitationally or hydrodynamically induced (for reviews see Boselli & Gavazzi 2006; Treu et al. 2003). Since only a small fraction of the galaxies studied are probably located in rich clusters, we have not sought to consider processes that occur primarily in such very high density environments. Improbable processes are ram pressure stripping, consisting of the gas stripping of a galaxy moving through a dense inter-galactic medium and the abrupt truncation of its star formation, and harassment, i.e. a gravitational interaction in high velocity encounters of galaxies, causing morphological transformation and bursts of star formation. Given the typical galaxy velocities and inter-galactic medium density involved in these processes, they cannot have a significant impact on the results presented in this paper. Post-starburst galaxies have been found in a wide range of environments in DEEP2 (Yan et al. 2009) and zCOSMOS (Vergani et al. 2010) indicating that the formation mechanism behind this class

of objects, i.e. their star formation shutdown, is not a peculiarity of clusters.

Viable mechanisms in the field are galaxy-galaxy merging and starvation. Major merging processes can trigger AGN activity and quench the star formation: the fraction of pairs, related to the rate of merging, may depend on environment. Merging of galaxies in the densest regions is impeded by the high relative velocities, but at high redshift, supposedly $z \sim 1$, this process was more common, thus the merging rate higher (de Ravel et al. 2009). In this context, at high redshift merging processes produced a shift in the GSMF towards higher masses, because of the depletion at low masses and consequent increase in early-type galaxies at high masses. At later times, the decrease in the merging rate ensures that the high mass end remains almost constant, while the acquisition of new galaxies from the field, by means of the hierarchical growth of the structures, can produce the observed shape of the D4 GSMF at low redshift in Figs. 3 and 4, the dip at intermediate masses, and the high contribution of massive early-type galaxies.

To explain the evolution in the density of massive elliptical galaxies, Ilbert et al. (2010) concluded that the rate of wet mergers should steeply decline at $z < 1$. Limits on the contribution of major merging as primary mechanism can be drawn from the evolution of pair fraction (de Ravel et al. 2009, who found that 20% of the stellar mass in present day galaxies with $\log \mathcal{M}/\mathcal{M}_\odot > 9.5$ has been accreted by major merging events since $z \sim 1$) and from the GSMF (Pozzetti et al. 2010, who derived an average number of total mergers $\sim 0.16\,\mathrm{gal}^{-1}\,\mathrm{Gyr}^{-1}$ since $z \sim 1$ for the global population, derived from the GSMF evolved according to the mass growth due to star formation).

In addition, strangulation (also referred to starvation or suffocation), consisting of halo-gas stripping, can play a role: when the diffuse warm and hot gas reservoir in the galaxy corona is stripped because of gravitational interaction with low-mass group-size haloes or with cluster haloes at large distances from the core, the gas cannot be accreted anymore and the galaxy will exhaust the remaining cold gas through star formation, on a timescale which can be instantaneous or slow, i.e., up to a few Gyr, depending on the mass of the galaxy (Wolf et al. 2009). The result is the suppression of the star formation, not immediately followed by a morphological transformation, explaining the possible presence of red spirals, even if the fading of the disc can lead to an earlier-type morphological classification. This mechanism alone is not able to reproduce the shape of the D4 GSMF and the contribution of the different galaxy types, since it predict a large amount of red galaxies at low masses (for the difficulties of the starvation scenario see also Bundy et al. 2010), as demonstrated by comparing observed data with simulations in Sect. 5.3; nonetheless, this mechanism may be effective in the group environment, where galaxies are undergoing morphological transformations and suppression of their star formation (e.g. Wilman et al. 2009).

To help identify the most likely transformation mechanisms, we also computed GSMFs for samples divided following the morphological classification by Scarlata et al. (2007), as defined in Sect. 2.5. In Fig. 9, we show the values of $\mathcal{M}_{\rm cross}$ in the 4 considered redshift bins. This plot appears to differ from the analogous plot obtained for samples produced by dividing galaxies on the basis of photometric types: the values of $\mathcal{M}_{\rm cross}$ are higher and their evolution seems insensitive to the environment from $z \sim 1$ to $z \sim 0.4$. The higher values of $\mathcal{M}_{\rm cross}$ for the morphological classification suggest that the dynamical transformation into elliptical galaxies follows the quenching of their star formation. It is possible that the transformations of morphology

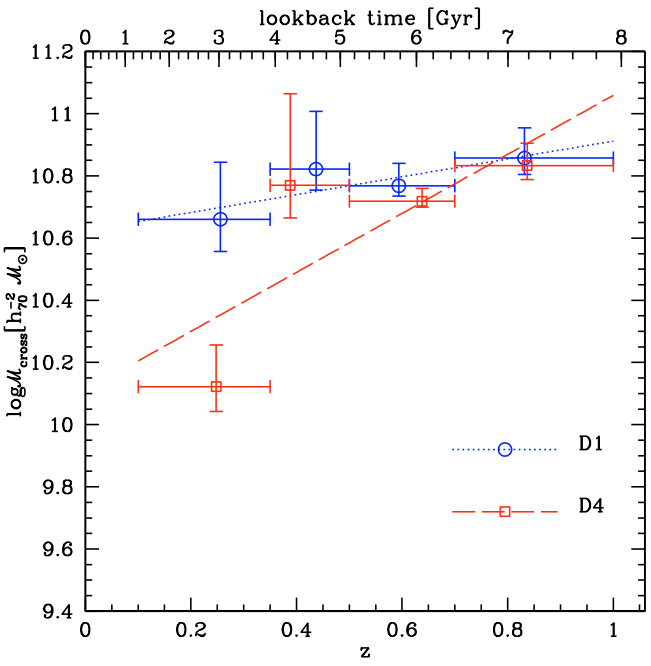

Fig. 9. Like Fig. 7, with $\mathcal{M}_{\rm cross}$ computed for morphological types.

occur on longer timescales than those of colour (e.g., Capak et al. 2007a; Smith et al. 2005; Bamford et al. 2009; Wolf et al. 2009), as inferred also from the study of post-starburst galaxies selected in the same zCOSMOS sample (Vergani et al. 2010) or by considering different evolutionary paths (Skibba et al. 2009). A more comprehensive study should be performed to investigate this point, since the larger number of photometric early-types than morphological ones may also be caused by a relatively large fraction of dust-reddened spiral galaxies.

To evaluate the uncertainties related to this comparison of photometric and morphological types, we altered the threshold between elliptical galaxies and morphological late-types: we divided the morphological class 2.1, which should still represent bulge-dominated galaxies, following the observed $B-z$: the evolutionary track of the $B-z$ colour of a galaxy Sab (Coleman et al. 1980) provides a criterion to separate quiescent and star-forming galaxies in good agreement with the spectral classification, as shown in Mignoli et al. (2009). With this separation, the values of the morphological $\mathcal{M}_{\rm cross}$ become consistent with the photometric values, both in terms of the absolute value and the trend with redshift.

Both mechanisms, gas stripping and interactions, likely operate to explain the suppression of the star formation and the morphological transformation. Those processes act on different timescales and have different efficiencies as a function of galaxy mass and environment, but it is still difficult to draw firm conclusions, because of the uncertainties associated with the galaxy classification.

5.3. Comparison with mock catalogues

We used 12 COSMOS mock lightcones (Kitzbichler & White 2007) based on the Millennium N-body simulation (Springel et al. 2005). The galaxy population of lightcones was then assigned by means of semi-analytical recipes (Croton et al. 2006; De Lucia & Blaizot 2007). The final catalogues are the same as

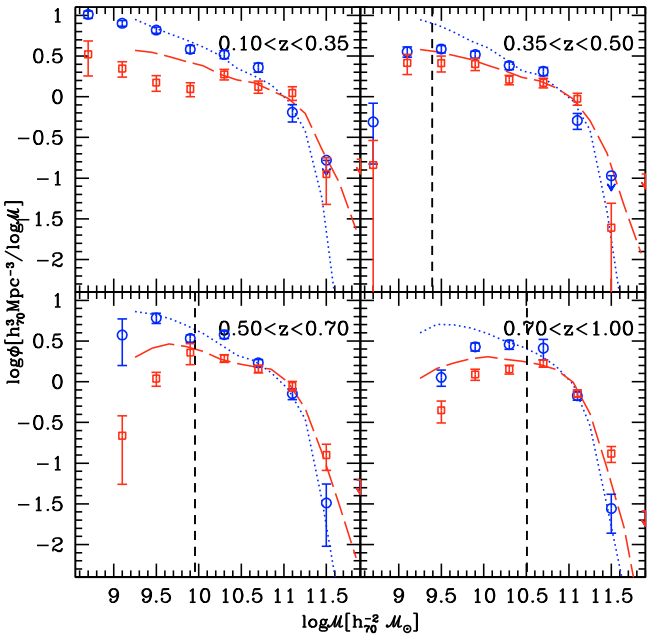

Fig. 10. GSMFs derived with $1/V_{max}$ method in mock catalogues (D1 environment: blue dotted lines, D4: red dashed lines, both representing the average obtained from 12 mocks) compared to the observed ones (points) in D1 and D4 environments (blue circles and red squares, respectively). The functions are rescaled to arbitrary units, to maintain the same integral of the GSMFs in the overdense regions at masses larger than $10^{10.5}$ $\mathcal{M}_\odot$ in observed and mocks samples.

those described in Knobel et al. (2009), who used them to test the group finder algorithm.

We used the 5NN flux-limited $1+\delta$ estimate of the environment and the rest-frame colour $B-I$ to differentiate early- from late-type galaxies, and to be able to compare the same quantities in observations and mocks. Even though at the lowest stellar masses the mock catalogues may be affected by colour incompleteness, this does not affect our analysis, since we limit our comparison to the higher masses probed in the zCOSMOS. In Fig. 10, we compare the high and low-density GSMFs in both the observed sample and the 12 averaged mock catalogues. To avoid normalisation uncertainties caused by cosmic variance (Meneux et al. 2009), we decided to renormalise the GSMFs, in such a way that the observed and mock GSMFs of the overdense regions have the same integral value at masses higher than $10^{10.5}$ $\mathcal{M}_\odot$ in all the redshift bins. The most evident characteristic of the observed GSMFs, namely the bimodality of the GSMFs in overdense regions at low redshift, is not reproduced by semi-analytical models. To explore the reason for this failure of semi-analytical models (SAMs) in reproducing observations, we separated red and blue galaxies adopting the threshold $B-I=1.15$, which corresponds to the location of the dip of the colour bimodality, obtaining the GSMFs in Fig. 11. For the low density environments, SAMs produce too many blue galaxies at intermediate and especially at high masses in all the redshift bins, and consequently also a too low density of red galaxies, in particular at 10^{10}–10^{11} $\mathcal{M}_\odot$. This can be ascribed to an inefficient suppression of the star formation in the absence of external drivers, as in the case of sparse environments. Weinmann et al. (2006) also find a too high blue fraction of central galaxies: they explain this discrepancy by an improper modelling of dust extinction, which is very likely underestimated for starburst galaxies, and AGN feedback, that may be more effective above a given halo mass. A threshold halo mass above which the star formation is naturally shut down, as proposed by Cattaneo et al. (2008), may also alleviate the discrepancy.

In the high density regions, the most visible difference is the excess of low and intermediate mass red galaxies ($<10^{10}$ $\mathcal{M}_\odot$) in SAMs with respect to the observed fractions in the lowest redshift bin, where the probed mass range is wider. This last comparison reflects the problem of the overquenching of satellites in the SAMs we used, which produces too many small red galaxies: a too efficient strangulation produces an instantaneous shut down of the star formation when a galaxy enters in a halo (see Weinmann et al. 2006, 2010; Font et al. 2008; Kang & van den Bosch 2008; Kimm et al. 2009; Fontanot et al. 2009, for a description of the problem and some attempts to solve it).

6. Conclusions

We have computed GSMFs in different environments and studied the relative contributions of different galaxy types to these GSMFs, and their evolution. Our main results are:

1. The bimodality seen in the global GSMF (Pozzetti et al. 2010) up to $z\sim0.5$ is considerably more pronounced in high density environments; a sum of two Schechter functions is thus required to reproduce the observed non-parametric estimates of the GSMF.
2. The bimodality is due to the different relative contributions of early- and late-type galaxies in different environments, each contribution being reasonably well represented by a single Schechter function.
3. The shapes of the GSMFs of different galaxy types in different environments and their evolution with time are very similar, i.e., the differences on the global GSMFs may be ascribed to the evolution in the normalisation of the GSMFs of different galaxy types in the extreme environments we have considered.
4. The evolution with time in the fractional contributions of different galaxy types to the environmental GSMF appears to be a function of the overdensity in which the galaxies live, and is consistent with a higher rate of downsizing with time in overdense regions.
5. The evolution of the crossover mass for photometric late- and early-type galaxies suggests a faster transition rate in overdense regions, with galaxies in low-density regions experiencing the same evolutionary path as the analogous galaxies in overdense environments with a delay of ~2 Gyr being accumulated between $z\sim1$ and $z\sim0.2$.
6. The environment starts to play a significant role in the evolution of galaxies at $z\lesssim1$.
7. The timescales for quenching of star formation and morphological metamorphosis differ in different environments; tentatively, the crossover mass considering morphological classification suggests that the morphological transformation is slower than the colour change.
8. SAMs fail in different ways as a function of the environment: GSMFs computed from mock catalogues show an underestimate of the number of red massive galaxies in low density environments, probably because of an inefficient internal mechanism suppressing the star formation at relatively high masses; in high density regimes the overquenching problem of satellites in SAMs causes an excess of red galaxies at intermediate and low masses.

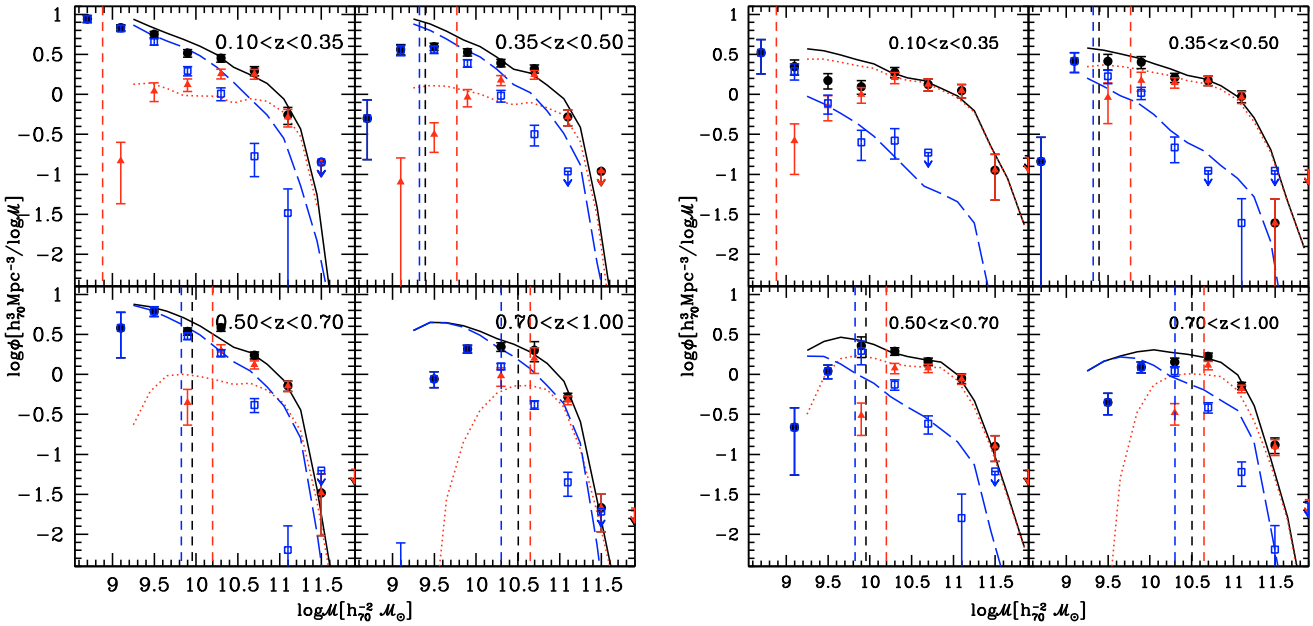

Fig. 11. *Left*: quartile D1 (low density environment). *Right*: quartile D4 (high density). Points refer to the observed quantities, lines to the GSMFs derived from the mock catalogues. Black points and solid lines: GSMFs relative to the considered density quartile, renormalised to the same integral at $\log \mathcal{M}/\mathcal{M}_{\odot} > 10.5$. Red triangles and dotted lines: galaxies with $B-I > 1.15$. Blue squares and dashed lines: galaxies with $B-I \leq 1.15$.

As a consequence of the remarkable difference in the shape of the GSMFs in under- and overdense regions, we can infer that all the galaxy properties depending on mass will also depend on environment by virtue of the GSMF environmental dependence, as shown in the case of the colour-density and morphology-density relations (Cucciati et al. 2010; Tasca et al. 2009) and of the AGN fraction (Silverman et al. 2009).

The nature versus nurture debate is unresolvable, because the mass of a galaxy, often thought to be its nature, is a strong function of the environment. A more relevant issue is the understanding of the mechanisms producing the observed evolution of galaxies and their transition from late- to early-type in different environments.

Future investigations will also concern the impact of merging in different environments (de Ravel et al. 2010; Kampczyk et al. 2010) and the role of the dark-matter halo mass functions in different environments (e.g. Abbas & Sheth 2007) in the determining galaxy formation efficiency.

Acknowledgements. M.B. wishes to thank Preethi Nair, Alexis Finoguenov, and Ramin Skibba for useful discussions, comments and suggestions. We thank the anonymous referee for the constructive first report, that helped improve the paper. M.B. is grateful to the editor, Françoise Combes, for her kind support.
This work was partly supported by an INAF contract PRIN/2007/1.06.10.08 and an ASI grant ASI/COFIS/WP3110 I/026/07/0.

References

Abbas, U., & Sheth, R. K. 2007, MNRAS, 378, 641
Avni, Y., & Bahcall, J. N. 1980, ApJ, 235, 694
Bañados, E., Hung, L., De Propris, R., & West, M. J. 2010, ApJ, 721, L14
Baldry, I. K., Glazebrook, K., Brinkmann, J., et al. 2004, ApJ, 600, 681
Baldry, I. K., Balogh, M. L., Bower, R. G., et al. 2006, MNRAS, 373, 469
Baldry, I. K., Glazebrook, K., & Driver, S. P. 2008, MNRAS, 388, 945
Balogh, M. L., Christlein, D., Zabludoff, A. I., & Zaritsky, D. 2001, ApJ, 557, 117
Balogh, M. L., Baldry, I. K., Nichol, R., et al. 2004, ApJ, 615, L101
Balogh, M. L., Wilman, D., Henderson, R. D. E., et al. 2007, MNRAS, 374, 1169
Balogh, M. L., McGee, S. L., Wilman, D., et al. 2009, MNRAS, 398, 754
Bamford, S. P., Nichol, R. C., Baldry, I. K., et al. 2009, MNRAS, 393, 1324
Bernardi, M., Nichol, R. C., Sheth, R. K., Miller, C. J., & Brinkmann, J. 2006, AJ, 131, 1288
Blanton, M. R., Eisenstein, D., Hogg, D. W., Schlegel, D. J., & Brinkmann, J. 2005a, ApJ, 629, 143
Blanton, M. R., Lupton, R. H., Schlegel, D. J., et al. 2005b, ApJ, 631, 208
Bolzonella, M., Miralles, J.-M., & Pelló, R. 2000, A&A, 363, 476
Boselli, A., & Gavazzi, G. 2006, PASP, 118, 517
Bottini, D., Garilli, B., Maccagni, D., et al. 2005, PASP, 117, 996
Bruzual, G., & Charlot, S. 2003, MNRAS, 344, 1000
Bundy, K., Ellis, R. S., Conselice, C. J., et al. 2006, ApJ, 651, 120
Bundy, K., Scarlata, C., Carollo, C. M., et al. 2010, ApJ, 719, 1969
Calzetti, D., Armus, L., Bohlin, R. C., et al. 2000, ApJ, 533, 682
Capak, P., Abraham, R. G., Ellis, R. S., et al. 2007a, ApJS, 172, 284
Capak, P., Aussel, H., Ajiki, M., et al. 2007b, ApJS, 172, 99
Cattaneo, A., Dekel, A., Faber, S. M., & Guiderdoni, B. 2008, MNRAS, 389, 567
Chabrier, G. 2003, PASP, 115, 763
Clemens, M. S., Bressan, A., Nikolic, B., et al. 2006, MNRAS, 370, 702
Coleman, G. D., Wu, C.-C., & Weedman, D. W. 1980, ApJS, 43, 393
Conroy, C., Gunn, J. E., & White, M. 2009, ApJ, 699, 486
Cooper, M. C., Newman, J. A., Madgwick, D. S., et al. 2005, ApJ, 634, 833
Cooper, M. C., Newman, J. A., Weiner, B. J., et al. 2008, MNRAS, 383, 1058
Cooper, M. C., Coil, A. L., Gerke, B. F., et al. 2010a, MNRAS, 1317
Cooper, M. C., Gallazzi, A., Newman, J. A., & Yan, R. 2010b, MNRAS, 402, 1942
Croton, D. J., Springel, V., White, S. D. M., et al. 2006, MNRAS, 365, 11
Cucciati, O., Iovino, A., Kovac, K., et al. 2010, A&A, 524, A2
Cucciati, O., Iovino, A., Marinoni, C., et al. 2006, A&A, 458, 39
Davis, M., Faber, S. M., Newman, J., et al. 2003, in SPIE Conf. Ser. 4834, ed. P. Guhathakurta, 161
De Lucia, G., & Blaizot, J. 2007, MNRAS, 375, 2
de Ravel, L., Le Fèvre, O., Tresse, L., et al. 2009, A&A, 498, 379
de Ravel, L., Kampczyc, P., & zCOSMOS collaboration. 2010, A&A, submitted
Desai, V., Dalcanton, J. J., Aragón-Salamanca, A., et al. 2007, ApJ, 660, 1151
Dressler, A. 1980, ApJ, 236, 351
Drory, N., Bundy, K., Leauthaud, A., et al. 2009, ApJ, 707, 1595
Elbaz, D., Daddi, E., Le Borgne, D., et al. 2007, A&A, 468, 33
Feldmann, R., Carollo, C. M., Porciani, C., et al. 2006, MNRAS, 372, 565
Feldmann, R., Carollo, C. M., Porciani, C., Lilly, S. J., & Oesch, P. 2008, [arXiv:0801.3275]
Finoguenov, A., Guzzo, L., Hasinger, G., et al. 2007, ApJS, 172, 182
Font, A. S., Bower, R. G., McCarthy, I. G., et al. 2008, MNRAS, 389, 1619
Fontana, A., Pozzetti, L., Donnarumma, I., et al. 2004, A&A, 424, 23

Fontanot, F., De Lucia, G., Monaco, P., Somerville, R. S., & Santini, P. 2009, MNRAS, 397, 1776
Gallazzi, A., Bell, E. F., Wolf, C., et al. 2009, ApJ, 690, 1883
Garilli, B., Fumana, M., Franzetti, P., et al. 2010, PASP, 122, 827
Gavazzi, G., Fumagalli, M., Cucciati, O., & Boselli, A. 2010, A&A, 517, A73
Gehrels, N. 1986, ApJ, 303, 336
Gómez, P. L., Nichol, R. C., Miller, C. J., et al. 2003, ApJ, 584, 210
Hogg, D. W., Blanton, M. R., Eisenstein, D. J., et al. 2003, ApJ, 585, L5
Ilbert, O., Tresse, L., Arnouts, S., et al. 2004, MNRAS, 351, 541
Ilbert, O., Tresse, L., Zucca, E., et al. 2005, A&A, 439, 863
Ilbert, O., Arnouts, S., McCracken, H. J., et al. 2006, A&A, 457, 841
Ilbert, O., Capak, P., Salvato, M., et al. 2009, ApJ, 690, 1236
Ilbert, O., Salvato, M., Le Floc'h, E., et al. 2010, ApJ, 709, 644
Iovino, A., Cucciati, O., Scodeggio, M., et al. 2010, A&A, 509, A40
Jenkins, L. P., Hornschemeier, A. E., Mobasher, B., Alexander, D. M., & Bauer, F. E. 2007, ApJ, 666, 846
Just, D. W., Zaritsky, D., Sand, D. J., Desai, V., & Rudnick, G. 2010, ApJ, 711, 192
Kampczyk, P., & zCOSMOS collaboration. 2010, ApJ, submitted
Kang, X., & van den Bosch, F. C. 2008, ApJ, 676, L101
Kauffmann, G., Heckman, T. M., Tremonti, C., et al. 2003, MNRAS, 346, 1055
Kauffmann, G., White, S. D. M., Heckman, T. M., et al. 2004, MNRAS, 353, 713
Kimm, T., Somerville, R. S., Yi, S. K., et al. 2009, MNRAS, 394, 1131
Kinney, A. L., Calzetti, D., Bohlin, R. C., et al. 1996, ApJ, 467, 38
Kitzbichler, M. G., & White, S. D. M. 2007, MNRAS, 376, 2
Knobel, C., Lilly, S. J., Iovino, A., et al. 2009, ApJ, 697, 1842
Koekemoer, A. M., Aussel, H., Calzetti, D., et al. 2007, ApJS, 172, 196
Kovač, K., Lilly, S. J., Cucciati, O., et al. 2010a, ApJ, 708, 505
Kovač, K., Lilly, S. J., Knobel, C., et al. 2010b, ApJ, 718, 86
Kroupa, P. 2001, MNRAS, 322, 231
Le Fèvre, O., Vettolani, G., Maccagni, D., et al. 2003, in SPIE Conf. Ser. 4834, ed. P. Guhathakurta, 173
Lee, J. H., Lee, M. G., Park, C., & Choi, Y. 2010, MNRAS, 403, 1930
Lilly, S. J., Le Fèvre, O., Renzini, A., et al. 2007, ApJS, 172, 70
Lilly, S. J., Le Brun, V., Maier, C., et al. 2009, ApJS, 184, 218
Lin, L., Koo, D. C., Weiner, B. J., et al. 2007, ApJ, 660, L51
Maier, C., Lilly, S. J., Zamorani, G., et al. 2009, ApJ, 694, 1099
Maraston, C. 2005, MNRAS, 362, 799
Maraston, C., Daddi, E., Renzini, A., et al. 2006, ApJ, 652, 85
Marchesini, D., van Dokkum, P. G., Förster Schreiber, N. M., et al. 2009, ApJ, 701, 1765
Marigo, P., & Girardi, L. 2007, A&A, 469, 239
Mateus, A., Sodré, L., Cid Fernandes, R., & Stasińska, G. 2007, MNRAS, 374, 1457
Mateus, A., Jimenez, R., & Gaztañaga, E. 2008, ApJ, 684, L61
McCracken, H. J., Capak, P., Salvato, M., et al. 2010, ApJ, 708, 202
Meneux, B., Guzzo, L., de La Torre, S., et al. 2009, A&A, 505, 463
Mignoli, M., Zamorani, G., Scodeggio, M., et al. 2009, A&A, 493, 39
Moresco, M., Pozzetti, L., Cimatti, A., et al. 2010, accepted
Oesch, P. A., Carollo, C. M., Feldmann, R., et al. 2010, ApJ, 714, L47
Panter, B., Heavens, A. F., & Jimenez, R. 2004, MNRAS, 355, 764
Patel, S. G., Holden, B. P., Kelson, D. D., Illingworth, G. D., & Franx, M. 2009a, ApJ, 705, L67
Patel, S. G., Kelson, D. D., Holden, B. P., et al. 2009b, ApJ, 694, 1349
Peng, Y., Lilly, S. J., Kovač, K., et al. 2010, ApJ, 721, 193
Poggianti, B. M., Smail, I., Dressler, A., et al. 1999, ApJ, 518, 576
Poggianti, B. M., Fasano, G., Bettoni, D., et al. 2009, ApJ, 697, L137
Popesso, P., Biviano, A., Böhringer, H., & Romaniello, M. 2006, A&A, 445, 29
Popesso, P., Biviano, A., Böhringer, H., & Romaniello, M. 2007, A&A, 464, 451
Pozzetti, L., Bolzonella, M., Lamareille, F., et al. 2007, A&A, 474, 443
Pozzetti, L., Bolzonella, M., Zucca, E., et al. 2010, A&A, 523, A13
Rogers, B., Ferreras, I., Pasquali, A., et al. 2010, MNRAS, 405, 329
Rudnick, G., von der Linden, A., Pelló, R., et al. 2009, ApJ, 700, 1559
Salpeter, E. E. 1955, ApJ, 121, 161
Sánchez-Blázquez, P., Jablonka, P., Noll, S., et al. 2009, A&A, 499, 47
Sargent, M. T., Carollo, C. M., Lilly, S. J., et al. 2007, ApJS, 172, 434
Scarlata, C., Carollo, C. M., Lilly, S., et al. 2007, ApJS, 172, 406
Schechter, P. 1976, ApJ, 203, 297
Scodeggio, M., Franzetti, P., Garilli, B., et al. 2005, PASP, 117, 1284
Scodeggio, M., Vergani, D., Cucciati, O., et al. 2009, A&A, 501, 21
Scoville, N., Aussel, H., Benson, A., et al. 2007a, ApJS, 172, 150
Scoville, N., Aussel, H., Brusa, M., et al. 2007b, ApJS, 172, 1
Silverman, J. D., Kovač, K., Knobel, C., et al. 2009, ApJ, 695, 171
Simard, L., Clowe, D., Desai, V., et al. 2009, A&A, 508, 1141
Skibba, R. A., Bamford, S. P., Nichol, R. C., et al. 2009, MNRAS, 399, 966
Smith, G. P., Treu, T., Ellis, R. S., Moran, S. M., & Dressler, A. 2005, ApJ, 620, 78
Spaenhauer, A. M. 1978, A&A, 65, 313
Springel, V., White, S. D. M., Jenkins, A., et al. 2005, Nature, 435, 629
Tanaka, M., Goto, T., Okamura, S., Shimasaku, K., & Brinkmann, J. 2004, AJ, 128, 2677
Tasca, L. A. M., Kneib, J., Iovino, A., et al. 2009, A&A, 503, 379
Thomas, D., Maraston, C., Schawinski, K., Sarzi, M., & Silk, J. 2010, MNRAS, 404, 1775
Trentham, N. 1998, MNRAS, 294, 193
Trentham, N., Sampson, L., & Banerji, M. 2005, MNRAS, 357, 783
Treu, T., Ellis, R. S., Kneib, J.-P., et al. 2003, ApJ, 591, 53
van den Bosch, F. C., Aquino, D., Yang, X., et al. 2008a, MNRAS, 387, 79
van den Bosch, F. C., Pasquali, A., Yang, X., et al. 2008b, MNRAS, submitted [arXiv:0805.0002]
van der Wel, A., Rix, H., Holden, B. P., Bell, E. F., & Robaina, A. R. 2009, ApJ, 706, L120
van der Wel, A., Bell, E. F., Holden, B. P., Skibba, R. A., & Rix, H. 2010, ApJ, 714, 1779
Vergani, D., Zamorani, G., Lilly, S., et al. 2010, A&A, 509, A42
Weinmann, S. M., van den Bosch, F. C., Yang, X., et al. 2006, MNRAS, 372, 1161
Weinmann, S. M., Kauffmann, G., van den Bosch, F. C., et al. 2009, MNRAS, 237
Weinmann, S. M., Kauffmann, G., von der Linden, A., & De Lucia, G. 2010, MNRAS, 406, 2249
Welikala, N., Connolly, A. J., Hopkins, A. M., & Scranton, R. 2009, ApJ, 701, 994
Wilman, D. J., Oemler, A., Mulchaey, J. S., et al. 2009, ApJ, 692, 298
Wilman, D. J., Zibetti, S., & Budavári, T. 2010, MNRAS, 406, 1701
Wolf, C., Aragón-Salamanca, A., Balogh, M., et al. 2009, MNRAS, 393, 1302
Yan, R., Newman, J. A., Faber, S. M., et al. 2009, MNRAS, 398, 735
Zucca, E., Pozzetti, L., & Zamorani, G. 1994, MNRAS, 269, 953
Zucca, E., Zamorani, G., Vettolani, G., et al. 1997, A&A, 326, 477
Zucca, E., Ilbert, O., Bardelli, S., et al. 2006, A&A, 455, 879
Zucca, E., Bardelli, S., Bolzonella, M., et al. 2009, A&A, 508, 1217

[1] INAF – Osservatorio Astronomico di Bologna, via Ranzani 1, 40127 Bologna, Italy
e-mail: micol.bolzonella@oabo.inaf.it
[2] ETH Zurich, Institute of Astronomy, Wolfgang-Pauli-Straße 27, 8093 Zurich, Switzerland
[3] Laboratoire d'Astrophysique de Marseille, Université d'Aix-Marseille, CNRS, 38 rue Frédéric Joliot-Curie, 13388 Marseille Cedex 13, France
[4] INAF – Osservatorio Astronomico di Brera, via Brera 28, 20121 Milano, Italy
[5] INAF – IASF Milano, via Bassini 15, 20133 Milano, Italy
[6] Laboratoire d'Astrophysique de Toulouse-Tarbes, Université de Toulouse, CNRS, 14 avenue Édouard Belin, 31400 Toulouse, France
[7] Institute for Astronomy, Royal Observatory, Blackford Hill, Edinburgh, EH9 3HJ, Scotland, UK
[8] INAF – Osservatorio Astronomico di Torino, 10025 Pino Torinese (TO), Italy
[9] European Southern Observatory, Karl-Schwarzschild-Straße 2, 85748 Garching bei München, Germany
[10] INAF – Osservatorio Astronomico di Padova, vicolo dell'Osservatorio 5, 35122 Padova, Italy
[11] Max-Planck-Institut für Extraterrestrische Physik, Giessenbachstraße, 84571 Garching bei München, Germany
[12] Dipartimento di Astronomia, Università di Bologna, via Ranzani 1, 40127 Bologna, Italy
[13] Instituto de Astrofisica de Andalucia, CSIC, Apdo. 3004, 18080 Granada, Spain
[14] Instituto de Astrofisica de Canarias, vía Láctea s/n, 38205, La Laguna, Tenerife, Spain
[15] Institute for the Physics and Mathematics of the Universe (IPMU), University of Tokyo, Kashiwanoha 5-1-5, Kashiwa-shi, Chiba 277-8568, Japan
[16] University of Massachusetts, Amherst, USA
[17] Space Telescope Science Institute, 3700 San Martin Drive, Baltimore, MD 21218, USA
[18] LBNL & BCCP, University of California, Berkeley, CA 94720, USA
[19] Centre de Physique Théorique, UMR 6207 CNRS, Université de Provence, Case 907, 13288 Marseille, France
[20] Institut d'Astrophysique de Paris, UMR 7095 CNRS, Université Pierre et Marie Curie, 98bis Boulevard Arago, 75014 Paris, France
[21] Universitäts-Sternwarte, Scheinerstraße 1, 81679 München, Germany
[22] Argelander-Institut für Astronomie, Auf dem Hügel 71, 53121 Bonn, Germany
[23] INAF - Osservatorio Astronomico di Roma, via di Frascati 33, 00040 Monteporzio Catone, Italy
[24] DSM/Irfu/Service d'Astrophysique, CEA Saclay, 91191 Gif-sur-Yvette, France
[25] California Institute of Technology, MC 105-24, 1200 East California Boulevard, Pasadena, CA 91125, USA
[26] INAF – Osservatorio Astronomico di Arcetri, Largo E. Fermi 5, 50125 Firenze, Italy
[27] Institute for Astronomy, 2680 Woodlawn Drive, University of Hawaii, Honolulu, HI 96822, USA
[28] National Optical Astronomy Observatory, 950 North Cherry Avenue, Tucson, AZ 85719, USA
[29] Max Planck Institut für Plasma Physics and Excellence Cluster Universe, Boltzmannstraße 2, 85748 Garching bei München, Germany
[30] Research Center for Space and Cosmic Evolution, Ehime University, Bunkyo-cho, Matsuyama 790-8577, Japan
[31] Large Binocular Telescope Observatory, University of Arizona, 933 N. Cherry Ave., Tucson, AZ 85721-0065, USA